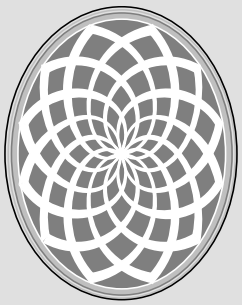

Interdisciplinary Mathematics Institute

2014:06

3-D Numerical Simulations of Biofilm Dynamics with Quorum Sensing in a Flow Cell

Jia Zhao and Qi Wang

IMI

Preprint Series

College of Arts and Sciences

University of South Carolina

3-D Numerical Simulations of Biofilm Dynamics with Quorum Sensing in a Flow Cell

Jia Zhao*and Qi Wang†

Abstract

Biofilms are microorganisms, where bacteria are embedded in networks formed by bacteria-produced expopolysacharrides, also known as extracellular polymeric substances (EPS). Bacteria in biofilms communicate and cooperate with each other by sensing the density of signalling molecules that bacteria excrete. This phenomenon is known as quorum sensing (QS). In this paper, we develop a hydrodynamic model for biofilms to include quorum sensing in biofilm dynamics, extending previous models for biofilms. In the new model, we classify bacteria into down-regulated and up-regulated quorum sensing cells, as well as non quorum sensing cells based on their quorum sensing ability. We then develop a numerical simulation tool for studying biofilms under quorum sensing in an aqueous environment by solving the hydrodynamic model in full 3D in space and time. Our numerical results show that this model captures key features of quorum sensing regulation that are responsible for the development of heterogeneous biofilm structures. For instance, numerical simulations with the model show that quorum sensing is beneficial for the biofilm development in a long run by building a robust EPS population to protect the biofilm, but maybe of little benefit in some short time frame because it slows down the development of biofilm colonies. In addition, numerical simulations demonstrate that quorum sensing induction in biofilms is sensitive to the hydrodynamic stress and competes directly with the nutrient supply. When nutrient supply is strong in the entire domain, QS induction produce more QS up-regulated bacteria to grow robust biofilm colonies upstream. On the other hand, when nutrient supply is weak, QS induction is more prominent downstream. Hydrodynamic stress also alters morphology of the biofilm when the flow is strong in the domain.

1 Introduction

Bacteria are ubiquitous in nature as well as in our daily life. In general, bacteria usually do not exist as isolated cells but rather live in organized communities. These bacterial communities, where bacteria are less motile and are glued together by exopopolysacharrides or extra cellular substances (EPS), are called biofilms. It's commonly perceived by the medical community that biofilms are responsible for many diseases or ailments associated with chronic infections, supported by the survey data that biofilms are present on the removed tissue of 80% of patients undergoing surgery for chronic sinusitis [**?**]. Unlike a planktonic (free-swimming) bacterium, bacteria in biofilms appear to be more adaptive to the stressful environment, for instance, they are more tolerable to antimicrobial agents and hydrodynamic stress. As the result, biofilms are always hard to be eradicated by standard antimicrobial treatment [**?**], which perhaps explains the tendency for relapse of chronic diseases or ailments caused by biofilms.

*Department of Mathematics, University of South Carolina, Columbia, SC 29208

†Email: qwang@math.sc.edu, Tel/Fax: 803-777-6268/803-777-3783, Department of Mathematics, University of South Carolina, Columbia, SC 29208, U. S. A.; School of Mathematics, Nankai University, Tianjin, 300071, P. R. China; Beijing Computational Science Research Center, Beijing, 100084, P. R. China

One of the main features of biofilms, which make bacteria in biofilms functioning quite different from planktonic bacteria, is that bacteria living in biofilms are observed to communicate, and, further more, cooperate with each other by secreting solution-dissolvable signalling molecules known as autoinducers [**?**]. For gram-negative bacteria, this particular molecule is acyl homoserine lactones (AHLs) [**?**]. Experimental results have shown that bacteria can sense the concentration of the signaling molecules secreted by bacteria in the surrounding and function cooperatively to accomplish certain tasks when the concentration of antoinducers reaches a threshold value [**?**]. This phenomenon is commonly known as quorum sensing (QS). The signalling molecule or the autoinducer is therefore called the quorum sensing molecule. This cell-cell communication system (via quorum sensing) has been observed in many bacterial systems, such as vibrio fischeri [**?**], where quorum sensing was first observed, Pseudomonas aeruginosa, Escherichia coli and so on. This approach allows unicellular microorganism to perform behavior like multicellular organism.

Quorum sensing has been shown to be responsible for mediating a variety of social activities in biofilms, which include the secretion of diverse byproducts, biofilm growth [**?**], swarming motility and virulence gene expressions [**?**]. For an overview of quorum sensing mechanism in biofilm formation and function and up-to-date advances, readers are referred to the work of Miller's [**?**] and Waters's [**?**]. In addition, some non-signaling properties of quorum sensing molecules have also been reported in the literature [**?**]. Especially, the phenomenon of quorum sensing regulating expopolysacharride production during biofilm formation has been reported widely in the literature [**?**, **?**, **?**].

EPS can be treated as the so-called 'public good' since its a shared resource that each individual bacterium can take advantage of, even if it is produced by other bacteria. However, how quorum sensing regulation affect the EPS production is not clearly resolved. Besides, in some bacterial systems, like Vibrio cholerae, the EPS production is suppressed when the density of autoinducer reaches its threshold value [**?**]; whereas in Pseudomonas aeruginosa, the EPS production would be facilitated once the quorum sensing is activated [**?**]. In addition, as the phenomenon involves transport of signaling molecules, the heterogenous structure in biofilm colonies and the solvent-biomass interaction can not be ignored, as they can affect the convection and diffusion rates of the signaling molecules transported as well as the morphology of biofilm colonies. This motivates us to develop a full 3D mathematical model to study how quorum sensing regulates biofilm formation and development as well as the pros and cons of quorum sensing in an aqueous environment where hydrodynamic interaction between the various biofilm components and the ambient fluid flow is important.

The induction of quorum sensing is usually observed at high bacterial cell volume fractions, where the concentration of QS molecules is accumulated to a certain threshold value. However, a high bacterial cell density does not necessarily induce quorum sensing since many other factors have been observed to contribute to this induction such as nutrient supplies, hydrodynamic shear stress [**?**] and the PH environment. Intuitively, a hydrodynamic flow may have a diluting effect on the signalling molecules, which then lead to a delay or even failure of QS induction by preventing QS molecules, like AHLs, from reaching a certain threshold value. For instance, in [**?**], the author claims that the amount of biomass required for the full QS induction of the population increases as the flow rate increases. On the other hand, coming with the inflow solvent, more essential substances, such as nutrient which fuels the production of QS molecules by bacteria, would be fresh in; thus hydrodynamic flow may lead to higher production of the signalling molecules and thereby facilitate QS induction. Little work has been done to analyze the correlations, not to mention taking the heterogenous structure factor of biofilms into account. This adequately serves as another motivation for us to develop a full 3D hydrodynamic biofilm model to study the hydrodynamic effect on quorum sensing.

In the literature, related with quorum sensing, some other factors have also been singled out for possible impact to biofilm development. For instance, recently, it has been verified that, except for cooperation, there probably exist cheaters in the bacterial population which exploit the signaling molecules produced by others [**?**]. Vermant's group observed that quorum sensing coordinated secretion of rhamnolipid acts as a surfactant, which leads to finger pattern formation in swimming bacteria aggregates [**?**]. With the ever-

increasing knowledge about quorum sensing, researchers are working on developing potential applications by taking advantage of this cell-cell communication mechanism. For an overview of applications of quorum sensing in biotechnology, readers are referred to [**?**]. One promising application is that it is probably more efficient to use anti-quorum sensing treatment than antibiotic agents in treating some biofilm infections, which is likely to pose a selective pressure for the development of resistant mutants [**?**].

Inspired by experimental findings, researchers have come up with some mathematical models to study biofilm formation and function, as well as related issues, such as the mechanism of quorum sensing and its contributions to biofilm structures and activities. Two review papers [**?**, **?**] have given an overview of current advances in mathematical modeling of biofilms. Concerning coupling biofilm growth with quorum sensing features, several mathematical models have been developed, some of which are cell-based [**?**], some are spatially homogeneous consisting of ordinary different equations, which are derived based on the mass-action principle [**?**] while others are models consisting of partial differential equations. In particular, John Ward derived a series of models for analyzing quorum sensing mechanisms in one space dimension [**?**, **?**]. Hermann derived a 2D partial differential equation model coupled with the Stokes flow [**?**] and later he extended this model [**?**] and proved its wellposedness [**?**]. In [**?**], the author proposed a 2D quorum sensing model and studied the shape of biofilms at the onset of the hydrodynamic shear. However, there is very little work on 3D hydrodynamics of biofilms and the ambient fluid environment available in the literature, which takes into account the spatial-temporal heterogeneous structure of biofilms as well as the hydrodynamic flow effects. This is perhaps mainly because of the mathematical complexity and computational challenges in resolving biofilms which are a truly 3D microorganism with highly heterogeneous spatial-temporal structures and complex dynamics.

In this paper, we develop a new full 3D hydrodynamic model for the mixture system consisting of biofilms and the ambient fluid, extending our previous phase-field model for biofilms of two and three effective components [**?**, **?**]. This model couples hydrodynamics of the biofilm-solvent mixture to the quorum sensing activity, as well as dynamics of nutrient and antimicrobial agents. Using this model, we aim to investigate biofilm formation regulated by quorum sensing in an aqueous environment under hydrodynamical flows and possibly antimicrobial treatment. A second order numerical scheme in both time and space based on finite difference methods is devised to solve the governing system of partial differential equations in the model. The numerical solver for the discretized equations is implemented on graphical processing units (GPUs) in a 3D cubic geometry in space and time.

The 3D numerical simulation tool is put in use to investigate the role of quorum sensing to the dynamics of various biomass components as well as to the entire biofilm colony. Given the complexity of the problem, we select a couple of important case studies to present in this paper. Firstly, we benchmark the model on two features of quorum sensing: the sensitivity of biofilm development to the threshold value of quorum sensing induction and the effect of the growth rate of the quorum sensing down regulated bacteria. The second case is chosen because after having conducted many numerical experiments on model parameters, we notice that the model is very sensitive to the growth rate of the QS down-regulated bacteria. Then, we apply the full 3D simulation tool to investigate the interaction between the hydrodynamics and quorum sensing regulation. Finally, we examine the impact of hydrodynamic stresses on biofilm morphology.

The rest of this paper is organized into four sections. In the second section, we present the detail of the derivation of the hydrodynamic phase field model for biofilms. Then, we design an efficient numerical solver for the governing partial differential equations in the model using semi-implicit finite difference schemes in the third section. In the fourth section, the numerical results and discussions are presented. In the last section, we conclude the study.

2 Mathematical model

In this section, we extend a previously developed hydrodynamic model for biofilms [**?**] to include the effect of quorum sensing among the various bacterial phenotypes classified based on their quorum sensing abilities. The biofilm, consisting of bacteria, EPS and solvent, is coarse-grained into a single fluid model with multi-components, in which different types of bacteria, EPS, as well as solvent are modeled effectively as separate fluid components. Quorum sensing molecules, nutrient and antibiotic agents are treated as phantom materials which exhibit chemical reactive effects without their mass and volume being considered. Treating a small amount of substances of such small molecules as phantom materials is an effective approximation to the complex mixture system given the minute contribution from these materials to the total mass and volume of the material system.

2.1 Basic notations

We study biofilms in a cubic domain Ω, where L_x, L_y, L_z represent the length in the x,y,z direction, respectively, i.e.,

$$\Omega = [0 \quad L_x] \times [0 \quad L_y] \times [0 \quad L_z].$$

Following our previous approach [**?**, **?**], we denote the volume fraction of the effective solvent and biomass as ϕ_s and ϕ_n, respectively. In biomass, we further divide it into EPS and bacteria, whose volume fractions are denoted by ϕ_p and ϕ_b, respectively. By definition, it follows that $\phi_n = \phi_p + \phi_b$. The incompressibility condition of the mixture system requires

$$\phi_s + \phi_p + \phi_b = 1. \tag{2.1}$$

Let $\rho_b, \mathbf{v}_b$, $\rho_p, \mathbf{v}_p$ and $\rho_s, \mathbf{v}_s$ be the density and velocity of the bacteria, EPS and solvent, respectively. Then the volume-averaged density and velocity for the mixture is denoted as

$$\rho = \phi_b\rho_b + \phi_p\rho_p + \phi_s\rho_s, \quad \mathbf{v} = \phi_b\mathbf{v}_b + \phi_p\mathbf{v}_p + \phi_s\mathbf{v}_s. \tag{2.2}$$

In the biofilm model, we classify the bacteria into four different phenotypes according to their responses to quorum sensing (QS) molecules [**?**, **?**]: QS down-regulated bacteria (QS^-), QS up-regulated bacteria (QS^+), non-QS bacteria (non-QS), as well as the dead bacteria, whose volume fractions are denoted by ϕ_{b1}, ϕ_{b2}, ϕ_{b3} and ϕ_{b4}, respectively. Hence, the volume fraction of the bacteria is given by the sum of the volume fractions of the four types:

$$\phi_b = \phi_{b1} + \phi_{b2} + \phi_{b3} + \phi_{b4}. \tag{2.3}$$

In biofilms, QS^- are the bacteria, which can convert into QS^+ once the concentration of QS molecules reaches a threshold value; whereas QS^+ are the bacteria, which can convert into QS^- when the concentration of QS molecules is lower than the threshold. In another word, QS^- bacteria belong to the wild phenotype of the bacteria and QS^+ bacteria represent the phenotype who has bonded QS molecules and certain activated gene transcription for enhanced EPS production and therefore reacts differently from its original phenotype. Non-QS bacteria represent those bacteria who are not affected by the concentration of quorum sensing molecules but may be regulated by other proteins in the biofilm. These non-quorum sensing bacteria could be regarded a phenotype, which do not prefer a social relation with other bacteria, or they may also be treated as a different type of bacteria, such as invaders. Dead bacteria are those who lose their vitality but are still attached in the biofilm.

In addition to the above bacterial phenotypes, we also keep track of the functional components whose mass and volume are omitted in the model, but their chemical effects are retained as their mass fractions are

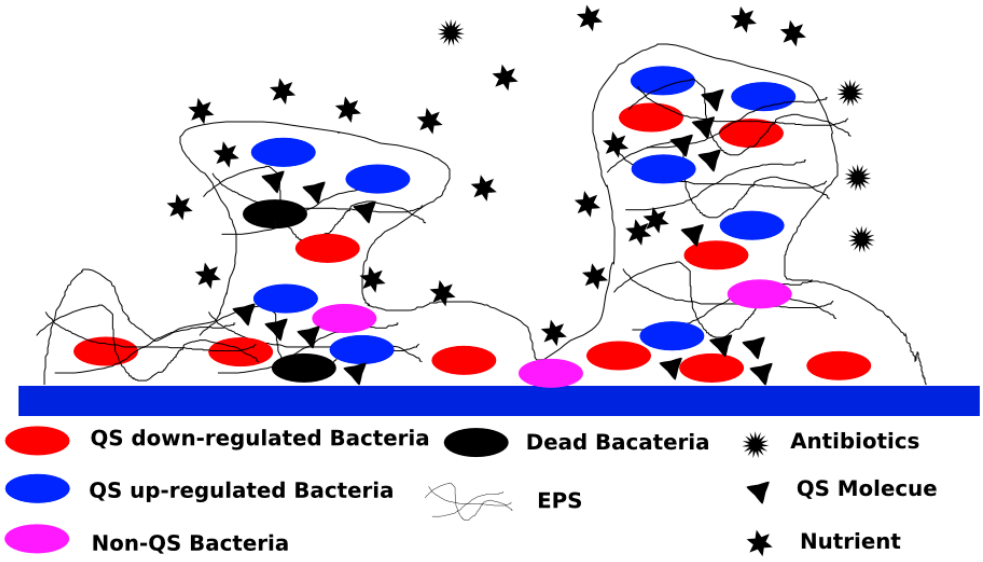

Figure 1: A Schematic cartoon for a biofilm colony with multiple components.

much smaller than those of the biomass and solvent. These are nutrients, antimicrobial agents and quorum sensing molecules, whose concentration are denoted by c, d and A, respectively. To help the reader better grasp the components in our model, we show a schematic cartoon for the biofilm colony in Figure **??**.

We make a simplifying assumption here that all bacterial cells and EPS that they produce interact with the solvent equally in terms of thermodynamics (entropic motion and mixing). Thus the effective free energy density functional of the biological system can be proposed as follows using the extended Flory-Huggin's mixing free energy density with an extra conformational entropy term [**?**]

$$f = k_B T\Big(\gamma_1\|\nabla\phi_n\|^2 + \gamma_2\left[\frac{\phi_n}{N}\log\phi_n + \phi_s\log\phi_s + \chi\phi_n\phi_s\right]\Big), \tag{2.4}$$

where k_B is the boltzmann constant, T is the absolute temperature, N is an effective polymerization index for the non-solvent biomass components, γ_1 parametrizes the strength of the conformational entropy, γ_2 parameterizes the strength of the bulk interaction potential, χ is the mixing coefficient. A more refined potential could be

$$f = k_B T\Big(\gamma_1\|\nabla\phi_n\|^2 + \gamma_2\left[\frac{\phi_n}{N_b}\log\phi_b + \frac{\phi_n}{N_p}\log\phi_p + \phi_s\log\phi_s + \chi\phi_n\phi_s\right]\Big), \tag{2.5}$$

where N_b and N_p are two effective polymerization index for the bacteria and EPS, respectively. In the problems we are interested in, the difference between the two potential is negligible. So, we adopt the simplified one in (**??**).

2.2 Transport equations for biomass components

With the proposed thermodynamic free energy, the transport equation for each bacterial cell type is assumed to be governed by a reactive Cahn-Hilliard type equation:

$$\frac{\partial\phi_{bj}}{\partial t} + \nabla\cdot(\mathbf{v}\phi_{bj}) = \nabla\cdot(\lambda_j\phi_{bj}\nabla\mu_j) + g_{bj}, \quad j = 1,2,3,4, \tag{2.6}$$

where λ_j is the mobility parameter for bacterial type j, $\mu_j = \frac{\delta f}{\delta \phi_{bj}}$ is the chemical potential with respect to bacterial type j, and g_{bj} is the reactive rate for cell type j.

The population dynamics of these cell types include regulated growth due to nutrient and decay due to antimicrobial agents as well as natural causes. Between the quorum sensing cells, there exists the up and down regulation coordinated by the concentration of the quorum sensing molecule AHL. The reactive kinetics for all cell types are given by

$$\begin{aligned}
g_{b1} &= (C_{b1}\phi_{b1} + \beta C_{b2}\phi_{b2})\tfrac{c}{k_b+c}\phi_{b1}(1-\tfrac{\phi_b}{\phi_{b,\max}}) - \tfrac{r_{12}A^n}{\tau^n+A^n}\phi_{b1} + \tfrac{r_{21}\tau^n}{A^n+\tau^n}\phi_{b2} - r_1\phi_{b1} - \tfrac{C_{d1}d}{k_{d1}+d}\phi_{b1},\\
g_{b2} &= (1-\beta)C_{b2}\tfrac{c}{k_b+c}\phi_{b2}(1-\tfrac{\phi_b}{\phi_{b,\max}}) + \tfrac{r_{12}A^n}{A^n+\tau^n}\phi_{b1} - \tfrac{r_{21}\tau^n}{A^n+\tau^n}\phi_{b2} - r_2\phi_{b2} - \tfrac{C_{d2}d}{k_{d2}+d}\phi_{b2},\\
g_{b3} &= \tfrac{C_{b3}c}{k_b+c}\phi_{b3}(1-\tfrac{\phi_b}{\phi_{b,\max}}) - r_3\phi_{b3} - \tfrac{C_{d3}d}{k_{d3}+d}\phi_{b3},\\
g_{b4} &= \textstyle\sum_{i=1}^3 r_i\phi_{bi} + \sum_{i=1}^3 \tfrac{C_{di}d}{k_{di}+d}\phi_{bi} - r_4\phi_{b4},
\end{aligned} \tag{2.7}$$

where the C_{bi} are the growth rates, β represents the percentage of QS^+ bacteria that produces QS^- bacteria, C_{di} is the decay rate due to the antimicrobial treatment, r_i is the natural death rate, k_{bi}, k_{di} are the half saturation constants in the respective Monod model for each bacterial phenotype, respectively, where $i = 1, 2, 3$. Here r_4 is the natural conversion rate from dead bacteria into solvent. In addition, $r_{12}\frac{A^n}{\tau^n+A^n}$ is the conversion rate from QS^- to QS^+, and $r_{21}\frac{\tau^n}{\tau^n+A^n}$ is the conversion rate from QS^+ to QS^-, $\phi_{b,max}$ is the carrying capacity for the bacterial volume fraction. τ is the threshold AHL concentration locally required for quorum sensing induction to occur. The exponent n describes the degree of polymerization in the synthesis of AHL, where we choose $n = 2$ in the study. When $A > \tau$, quorum sensing induction takes place to increase the up-regulated cell population and decrease the down-regulated cell population. The non-QS cells are not affected by the quorum sensing molecules by definition.

The transport equation for EPS (ϕ_p), which is the product of the live bacteria, is proposed as a reactive Cahn-Hilliard type equation as well and is given by,

$$\frac{\partial \phi_p}{\partial t} + \nabla\cdot(\mathbf{v}\phi_p) = \nabla\cdot(\lambda_p\phi_p\nabla\mu_p) + g_p, \tag{2.8}$$

where λ_p is the mobility parameter, $\mu_p = \frac{\delta f}{\delta \phi_p}$ is the chemical potential with respect to ϕ_p, and g_p is the reactive term proposed as follows

$$g_p = \sum_{i=1}^{3}\frac{C_{pi}c}{k_{pi}+c}\phi_{bi}\left(1-\frac{\phi_p}{\phi_{p,\max}}\right) + \alpha r_4\phi_{b4} - \frac{r_p k_{cp}}{k_{cp}+c}\phi_p - \frac{C_{dp}d}{k_{dp}+d}\phi_p. \tag{2.9}$$

Here C_{pj} is the EPS production rate with respect to the jth type cell, $j = 1, 2, 3$, facilitated by the nutrient. $\phi_{p,\max}$ gives the upper-bound for the EPS production. We assume a part of dead bacterial population is converted into EPS while others into the solvent, where α is the efficiency for the conversion, ranging between 0 and 1. We also assume that some EPS can be dissolved into the solvent naturally and accelerated by the drug with the rate given by r_p and C_{dp}, respectively. k_{pi}, k_{ap}, k_{cp} and k_{dp} are the half saturation constants for the Monod models adopted.

Because of the simplification assumption we made on the bacteria and EPS in the free energy, the chemical potential for each species is identical in this model. So the interfacial force due to the chemical potential to the momentum transport is given by

$$-\phi_n\nabla\mu_n = -\phi_p\nabla\mu_p - \sum_{j=1}^{4}\phi_{bj}\nabla\mu_{bj}. \tag{2.10}$$

With the proposed transport equations, we identify the transport velocity for bacteria, EPS and solvent, respectively, as follows:

$$\mathbf{v}_b = \mathbf{v} - \frac{1}{\phi_b}\sum_{i=1}^{4}\lambda_i\phi_{bi}\nabla\mu_n, \quad \mathbf{v}_p = \mathbf{v} - \lambda_p\nabla\mu_n, \quad \mathbf{v}_s = \frac{1}{\phi_s}[\mathbf{v} - \phi_p\mathbf{v}_p - \phi_b\mathbf{v}_b]. \tag{2.11}$$

where $\mu_n = \frac{\delta f}{\delta\phi_n}$ is the chemical potential for ϕ_n. Notice that the transport equation for ϕ_n can be derived by summing up the transport equation for each biomass component,

$$\frac{\partial\phi_n}{\partial t} + \nabla\cdot(\mathbf{v}\phi_n) = \nabla\cdot(\lambda\phi_n\nabla\mu_n) + g_p + \sum_{i=1}^{4} g_{bi}, \tag{2.12}$$

where $\lambda\phi_n = \sum_{i=1}^{4}\lambda_i\phi_i + \lambda_p\phi_p$. Since we need to keep track of each individual species in the model, this equation is not used in this model.

2.3 Transport equations for the functional components

There are three functional components in our biofilm model, namely, the nutrient, the antimicrobial agent, and the quorum sensing molecule, whose concentrations are denoted by c, d and A, respectively. These molecules all have small molecular weight compared with the components of the biomass, thus their molecular mass and volume are neglected in this model for simplicity. Instead of tracking their volumes, their concentrations are traced, which are governed by traditional convection-diffusion-reaction equations. These molecules are dissolved in solvent so that they are transported with the solvent.

Specifically, the transport equation for the concentration of the quorum sensing molecule AHL (A) is given by

$$\frac{\partial(\phi_s A)}{\partial t} + \nabla\cdot(\mathbf{v}_s\phi_s A) = \nabla\cdot(\phi_s D_a\nabla A) + g_a, \tag{2.13}$$

where D_a is the diffusion coefficient and g_a is the reactive term, proposed as

$$g_a = -r_a A + \left(\sum_{i=1}^{2}(r_{ai} + \frac{C_{ai}A}{k_{ai}+A})\phi_{bi}\right)\left(1 - \frac{A}{A_{\max}}\right) - \frac{C_a d}{k_{da}+d}A. \tag{2.14}$$

Here r_a is the decay rate of the AHL concentration due to binding with QS bacterial cells, r_{a1} and r_{a2} are the growth rate due to the down-regulated and up-regulated quorum sensing cells, respectively. C_{a1} and C_{a2} are growth rates, which take into account the effects that the concentration of AHL would affect the productivity of bacteria for AHL positively. Here $A_{\max}$ gives the upper-bound for the concentration of the auto-inducers. C_a is the decay rate of AHL due to antimicrobial agents and k_{da} is the half saturation constant. The diffusion coefficient is proposed by following the Hinson model [**?**],

$$D_a = D_{a0}\frac{1-\phi_b}{1+\frac{1}{2}\phi_b}\frac{\phi_s}{\phi_s + \frac{\phi_p}{D_{pr}}}, \tag{2.15}$$

where the first term on the right hand side represents the reduction effect due to the presence of bacteria while the second term is an empirical fitting accounting for the reduction effect due to the presence of EPS. Here D_{pr} is a model parameter fitted experimentally.

The transport equation for the nutrient is proposed as follows

$$\frac{\partial\phi_s c}{\partial t} + \nabla\cdot(\phi_s\mathbf{v}_s c) = \nabla\cdot(D_s\phi_s\nabla c) + g_c, \tag{2.16}$$

where D_s is the diffusion coefficient for nutrient transport and the reactive rate is given by

$$g_c = -\sum_{i=1}^{3} \frac{r_{bi} c}{k_{bi} + c} \phi_{bi} - \sum_{i=1}^{3} \frac{r_{pi} c}{k_{pi} + c} \phi_{bi}, \tag{2.17}$$

The first term in g_c represents the nutrient consumption due to bacteria metabolism and the second term represents the nutrient consumption due to the EPS production.

For the diffusion rate of the nutrient (D_c), which is primarily oxygen in this model, Stewart [**?**] suggests the diffusion rate in biofilms is around 75% than that in the pure solvent. Since the molecular weight of oxygen is relatively small, it is supposed to penetrate EPS and the membrane of cells equally. So we set the diffusion rate of oxygen in biofilms as follows

$$D_c = D_{c0} \frac{1 - (\phi_b + \phi_p)}{1 + \frac{1}{2}(\phi_b + \phi_p)}, \tag{2.18}$$

where the second term in the expression represents the reduction in diffusion due to the presence of the biomass.

Finally, the transport equation for antibiotic agents is proposed as follows

$$\frac{\partial(\phi_s d)}{\partial t} + \nabla \cdot (\phi_s \mathbf{v}_s d) = \nabla \cdot (D_d \phi_s \nabla d) + g_d, \tag{2.19}$$

where D_d is the diffusion rate of antimicrobial agents and

$$g_d = -\frac{d}{k_d + d} (\sum_{i=1}^{4} r_{di} \phi_{bi} + r_{dp} \phi_p) - r_d d, \tag{2.20}$$

is the reactive term. The antibiotic is assumed to be consumed by all bacterial cells and EPS at different rates. Here r_d represents the natural decay rate of antimicrobial agents. For the diffusion rate D_d, we also adopt the Hinson model [**?**]

$$D_d = D_{d0} \frac{1 - \phi_b}{1 + \frac{1}{2}\phi_b} \frac{\phi_s}{\phi_s + \frac{\phi_p}{D_{pr}}}. \tag{2.21}$$

In the derivation of these transport equations, we try to include as many biological and physical factors as possible which results in a large set of model parameters. Some of them can be measured or searched from the existing literature, while others are obtained either using our best guesses or calibrated against some experiments. Nevertheless, these effects are quantitatively present in the biofilm system.

2.4 Momentum and Continuity Equation

In order to couple the biofilm components to hydrodynamics, we need the governing equation for the averaged velocity $\mathbf{v}$. As we mentioned above, we treat this biological system as one fluid with multiple components. By assuming the fluid mixture as solenoidal, we impose the balance of linear momentum and conservation of mass as follows

$$\rho \left(\frac{\partial \mathbf{v}}{\partial t} + \mathbf{v} \cdot \nabla \mathbf{v} \right) = -\nabla p + \nabla \cdot \tau - \phi_n \nabla \mu_n \tag{2.22}$$

$$\nabla \cdot \mathbf{v} = 0, \tag{2.23}$$

where ρ is the averaged density, p is the hydrostatic pressure, τ is the extra stress and the last term is the interfacial force due to the inhomogeneity of biomass distribution, derived from the virtual work principle.

In this paper, we propose the mixture as an extended Newtonian fluid, then the extra stress tensor is given by

$$\tau = 2\eta_b\phi_b\mathbf{D}_b + 2\eta_p\phi_p\mathbf{D}_p + 2\eta_s\phi_s\mathbf{D}_s, \tag{2.24}$$

where η_b, η_p and η_s are the viscosity of bacteria, EPS and solvent, and $\mathbf{D}_b$, $\mathbf{D}_p$ and $\mathbf{D}_s$ are the rate of deformation tensor, correspondingly,

$$\mathbf{D}_b = \frac{1}{2}(\nabla\mathbf{v}_b + \nabla\mathbf{v}_b^T), \quad \mathbf{D}_p = \frac{1}{2}(\nabla\mathbf{v}_p + \nabla\mathbf{v}_p^T), \quad \mathbf{D}_s = \frac{1}{2}(\nabla\mathbf{v}_s + \nabla\mathbf{v}_s^T), \tag{2.25}$$

where $\mathbf{v}_b, \mathbf{v}_p, \mathbf{v}_s$ are the velocities for bacteria, EPS and solvent. Their expressions are given in equation (**??**).

2.5 Boundary Conditions

In order to simulate biofilms in a fixed domain, we need to impose boundary conditions for the governing partial differential equations, which mimic common situations for biofilms being cultured and observed in vitro. In this paper, we are interested in simulating biofilm flows in two special geometries, namely in petri dish or a flow cell, in full 3D space and time.

2.5.1 Boundary conditions for biofilms in an infinite long channel

To mimic the biofilm development in a culture dish, both x and z directions are assumed periodic. At boundaries in the y direction, no-flux boundary conditions are imposed for the biomass and functional components and no-slip boundary conditions are imposed for the velocity components, that's

$$\begin{aligned}
(i\mathbf{v}_s\phi_s - D_i\phi_s\nabla i)\cdot\mathbf{n}|_{y=0,L_y} &= 0, \quad i = c, d, A, &(2.26)\\
\nabla\phi_i\cdot\mathbf{n}|_{y=0,L_y} &= 0, \quad i = b1, b2, b3, b4, p, &(2.27)\\
(\mathbf{v}\phi_i - \lambda\phi_i\nabla\frac{\delta f}{\delta\phi_i})\cdot\mathbf{n}|_{y=0,L_y} &= 0, \quad i = b1, b2, b3, b4, p. &(2.28)
\end{aligned}$$

We also impose a nutrient feeding condition $c|_{y=L_y} = c_0$ in place of the zero-flux condition for the nutrient wherever there is a steady supply of nutrients through the boundary at $y = L_y$.

2.5.2 Boundary conditions for biofilms in a finite flow-cell

For the case of biofilms in a finitely long water channel, which we call it a flow cell, periodic boundary conditions are imposed in the z direction, and y direction is bounded by solid walls, that's no slip boundary conditions for the velocity $\mathbf{v}$ and no flux boundary conditions for the biomass and functional components are imposed,

$$\begin{aligned}
(i\mathbf{v}_s\phi_s - D_i\phi_s\nabla i)\cdot\mathbf{n}|_{y=0,L_y} &= 0, \quad i = c, d, A, &(2.29)\\
\nabla\phi_i\cdot\mathbf{n}|_{y=0,L_y} &= 0, \quad i = b1, b2, b3, b4, p, &(2.30)\\
(\mathbf{v}\phi_i - \lambda\phi_i\nabla\frac{\delta f}{\delta\phi_i})\cdot\mathbf{n}|_{y=0,L_y} &= 0, \quad i = b1, b2, b3, b4, p. &(2.31)
\end{aligned}$$

The channel is finite in the x-direction. So, there exist the inlet-outlet boundary conditions. The inlet velocity at $x = 0$ is given by

$$\mathbf{v}_0 = (p_0 y(1-y), 0, 0)\,, \tag{2.32}$$

where p_0 is a prescribed pressure gradient. Suppose that the solvent has already reached equilibrium when flowing out of the cell at $x = L_x$, we impose $\mathbf{v}_x = 0$ at the out-let boundary. For nutrient c, we impose

the feeding boundary is at $x = 0$ with a prescribed boundary condition $c = c_0(y)$ and $c_x = 0$ is assumed at $x = L_x$. For the biomass, we impose no-flux boundary condition in the x direction, which only applies to the situation where no biomass is flown in and out of the flow-cell,

$$(\mathbf{v}\phi_i - \lambda\phi_i\nabla\frac{\delta f}{\delta\phi_i}) \cdot \mathbf{n}|_{x=0,L_x} = 0, \quad j = b1, b2, b3, b4, p. \tag{2.33}$$

2.6 Nondimensionalization

We denote t_0 as the reference time scale, h the reference length scale, and c_0, d_0 and A_0 the characteristic concentration of the nutrient, antimicrobial agents and quorum sensing molecules, respectively. Then, we nondimensionalize the variables as follows,

$$\tilde{t} = \frac{t}{t_0}, \tilde{x} = \frac{x}{h}, \tilde{\mathbf{v}} = \frac{\mathbf{v}t_0}{h}, \tilde{\tau} = \frac{\tau t_0^2}{\rho_0 h^2}, \tilde{p} = \frac{pt_0^2}{\rho_0 h^2}, \tilde{c} = \frac{c}{c_0}, \tilde{d} = \frac{d}{d_0}.$$

The following dimensionless parameters then emerge,

$$\Lambda = \tfrac{\lambda\rho_0}{t_0}, \Gamma_1 = \tfrac{\gamma_1 kTt_0^2}{\rho_0 h^4}, \Gamma_2 = \tfrac{\gamma_2 kTt_0^2}{\rho_0 h^2}, Re_s = \tfrac{\rho_0 h^2}{\eta_s t_0}, Re_p = \tfrac{\rho_0 h^2}{\eta_p t_0}, Re_b = \tfrac{\rho_0 h^2}{\eta_b t_0}, \tilde{\rho} = \phi_s\tfrac{\rho_s}{\rho_0} + \phi_n\tfrac{\rho_n}{\rho_0}$$

$$\tilde{C}_{bi} = C_{bi}t_0, \tilde{r}_{bi} = r_{bi}t_0, \tilde{C}_{di} = C_{di}t_0, \tilde{C}_{ai} = C_{ai}t_0, \tilde{r}_i = r_i t_0, \tilde{r}_{di} = r_{di}t_0, i = 1, 2, 3.$$

$$\tilde{k_{bi}} = \tfrac{k_{bi}}{c_0}, \quad \tilde{k}_{di} = \tfrac{k_{di}}{d_0}, \tilde{k}_d = \tfrac{k_d}{d_0}, \tilde{k}_{ai} = \tfrac{k_{ai}}{A_0}, \tilde{k}_{pi} = \tfrac{k_{pi}}{c_0}, \quad i = 1, 2, 3.$$

$$\tilde{r}_{cp} = r_{cp}t_0, \quad \tilde{k}_{dp} = \tfrac{k_{dp}}{d_0}, \tilde{k}_{cp} = \tfrac{k_{cp}}{c_0}, \tilde{D}_i = \tfrac{D_i t_0}{h^2}, i = c0, d0, A0.$$

For simplicity, we drop the symbol ˜, the nondimentionalized equations in the hydrodynamic model for biofilms are summarized as follows:

$$\begin{cases} \rho\left(\frac{\partial\mathbf{v}}{\partial t} + \mathbf{v}\cdot\nabla\mathbf{v}\right) &= \nabla\cdot(\phi_b\tau_b + \phi_p\tau_p + \phi_s\tau_s) - \nabla p - \Gamma_1\nabla\cdot(\nabla\phi_n\nabla\phi_n), \\ \nabla\cdot\mathbf{v} &= 0, \\ \frac{\partial\phi_{bj}}{\partial t} + \nabla\cdot(\mathbf{v}\phi_{bj}) &= \nabla\cdot(\Lambda\phi_{bj}\nabla\mu_j) + g_{bj}, \quad j = 1, 2, 3, 4, \\ \frac{\partial\phi_p}{\partial t} + \nabla\cdot(\mathbf{v}_n\phi_p) &= \nabla\cdot(\Lambda\phi_p\nabla\mu_p) + g_p, \\ \frac{\partial\phi_s c}{\partial t} + \nabla\cdot(\phi_s\mathbf{v}_s c) &= \nabla\cdot(D_c\phi_s\nabla c) + g_c, \\ \frac{\partial\phi_s A}{\partial t} + \nabla\cdot(\mathbf{v}\phi_s A) &= \nabla\cdot(D_a\phi_s\nabla A) + g_a, \\ \frac{\partial\phi_s d}{\partial t} + \nabla(\phi_s\mathbf{v}_s d) &= \nabla\cdot(D_d\phi_s\nabla d) + g_d, \end{cases} \tag{2.34}$$

where the reactive terms are given by

$$\begin{cases} g_{b1} &= (C_{b1}\phi_{b1}+\beta C_{b2}\phi_{b2})\frac{c}{k_{b1}+c}(1-\frac{\phi_b}{\phi_{b,\max}})-\frac{r_{12}A^2}{\tau^2+A^n}\phi_{b1}+\frac{r_{21}\tau^n}{A^n+\tau^n}\phi_{b2}-(r_1+\frac{C_{d1}d}{k_{d1}+d})\phi_{b1},\\ g_{b2} &= (1-\beta)\frac{C_{b2}c}{k_{b2}+c}\phi_{b2}(1-\frac{\phi_b}{\phi_{b,\max}})+\frac{r_{12}A^n}{A^n+\tau^n}\phi_{b1}-\frac{r_{21}\tau^n}{A^n+\tau^n}\phi_{b2}-r_2\phi_{b2}-\frac{C_{d2}d}{k_{d2}+d}\phi_{b2},\\ g_{b3} &= \frac{C_{b3}c}{k_{b3}+c}\phi_{b3}(1-\frac{\phi_b}{\phi_{b,\max}})-r_3\phi_{b3}-\frac{C_{d3}d}{k_{d3}+d}\phi_{b3},\\ g_{b4} &= \sum_{i=1}^3 r_i\phi_{bi}+\sum_{i=1}^3\frac{C_{di}d}{k_{di}+d}\phi_{bi}-r_4\phi_{b4},\\ g_p &= \sum_{i=1}^3\frac{C_{pi}c}{k_{pi}+c}\phi_{bi}\left(1-\frac{\phi_p}{\phi_{p,\max}}\right)+\alpha r_4\phi_4-r_p\phi_p-\frac{C_{dp}d}{k_{dp}+d}\phi_p,\\ g_a &= -r_aA+\left(\sum_{i=1}^2(r_{ai}+\frac{C_{ai}A}{k_{ai}+A})\phi_{bi}\right)\left(1-\frac{A}{A_{\max}}\right)-\frac{C_ad}{k_{da}+d}A,\\ g_c &= -\sum_{i=1}^3\frac{r_{bi}c}{k_{bi}+c}\phi_{bi}-\sum_{i=1}^3\frac{r_{pi}c}{k_{pi}+c}\phi_{bi},\\ g_d &= -\frac{d}{k_d+d}(\sum_{i=1}^4 r_{di}\phi_{bi}+r_{dp}\phi_p)-r_dd. \end{cases} \tag{2.35}$$

3 Numerical methods and GPU implementation

For these coupled PDEs, we devise a numerical method to solve them. In each time step, we solve the momentum equation first using the extrapolated data for the biomass and functional components. Then with the updated velocity, we solve the Cahn-Hilliard equations and transport equations for functional components. We note that, in the following notation, any variable with overline $^{n+1}$ represents the second-order extrapolation from the n-1th and the nth to the $n+1$th step.

For the momentum equation, we use a modified Gauge-Uzawa method [**?**] to calculate the velocity. Recall that the momentum equation is given by

$$\rho(\frac{\partial\mathbf{v}}{\partial t}+\mathbf{v}\cdot\nabla\mathbf{v})=\nabla\cdot(\phi_b\tau_b+\phi_p\tau_p+\phi_s\tau_s)-[\nabla p+\Gamma_1\nabla\cdot(\nabla\phi_n\otimes\nabla\phi_n)]$$

By adding a second order term $-\frac{1}{R_{e_a}}\nabla^2\mathbf{v}$ on both sides, where R_{e_a} is a numerically chosen Reynolds number, we rewrite the momentum equation into

$$\rho(\frac{\partial\mathbf{v}}{\partial t}+\mathbf{v}\cdot\nabla\mathbf{v})-\frac{1}{R_{e_a}}\nabla^2\mathbf{v}=-\nabla p-\Gamma_1\nabla^2\phi_n\nabla\phi_n+\nabla\cdot(\phi_b\tau_b+\phi_p\tau_p+\phi_s\tau_s)-\frac{1}{R_{e_a}}\nabla^2\mathbf{v}$$

The modified Gauge-Uzawa method is given by three steps.

1. Prediction:

$$\begin{cases} \rho^{n+1}[\frac{3\mathbf{u}^{n+1}-4\mathbf{v}^n+\mathbf{v}^{n-1}}{2\delta t}]+\rho^{n+1}\overline{\mathbf{v}}^{n+1}\cdot\nabla\overline{\mathbf{v}}^{n+1}+\frac{1}{2}(\nabla\cdot(\rho^{n+1}\overline{\mathbf{v}}^{n+1}))\overline{\mathbf{v}}^{n+1},\\ +\frac{1}{R_{e_s}}\nabla s^n+\nabla p^n-\frac{1}{R_{e_a}}\nabla^2\mathbf{u}^{n+1}=\overline{\mathbf{R}}^{n+1}-\frac{1}{R_{e_a}}\nabla^2\overline{\mathbf{v}}^{n+1-\varepsilon},\\ \mathbf{u}^{n+1}\cdot\mathbf{n}|_{y=0,L_y}=0,\\ \mathbf{u}^{n+1}|_{x=0}=\mathbf{v}_0,\quad \mathbf{u}_x^{n+1}|_{x=L_x}=0, \end{cases}$$

2. Projection:

$$\begin{cases} -\nabla\cdot(\frac{1}{\rho^{n+1}}\nabla\psi^{n+1}) = & \nabla\cdot\mathbf{u}^{n+1}, \\ \frac{\partial\psi^{n+1}}{\partial n}|_{y=0,L_y} = & 0, \\ \frac{\partial\psi^{n+1}}{\partial n}|_{x=0,L_x} = & 0, \end{cases}$$

3. Correction:

$$\begin{cases} \mathbf{v}^{n+1} = & \mathbf{u}^{n+1} + \frac{1}{\rho^{n+1}}\nabla\psi^{n+1}, \\ s^{n+1} = & s^n - \nabla\cdot\mathbf{u}^{n+1}, \\ p^{n+1} = & p^n - \frac{3\psi^{n+1}}{2\delta t} + \frac{1}{R_{e_a}}s^{n+1}, \end{cases}$$

where

$$\overline{\mathbf{R}}^{n+1} = -\Gamma_1\nabla^2\overline{\phi}_n^{n+1}\nabla\overline{\phi}_n^{n+1} + \nabla\cdot(\overline{\phi}_n^{n+1}\overline{\tau}_n^{n+1} + \overline{\phi}_s^{n+1}\overline{\tau}_s^{n+1})$$

and $\varepsilon = 0.05$ is used to improve the stability of the scheme. The numerically chosen Reynolds number R_{e_a} is computed by

$$\frac{1}{R_{e_a}} = \frac{\phi_{b,\max}}{R_{e_b}} + \frac{\phi_{p,\max}}{R_{e_p}} + \frac{1-\phi_{p,\max}-\phi_{b,\max}}{R_{e_s}},$$

Where R_{e_b}, R_{e_p} and R_{e_s} are the Reynolds numbers for bacteria, EPS and solvent, respectively. Here, we note that $s^0 = 0$ and $\mathbf{v}^1, s^1, \phi_i^1, i = b1, b2, b3, b4, p$ and c^1, d^1, A^1 are computed by a first order scheme without extrapolation.

For the Cahn-Hilliard equations, we use a semi-implicit finite difference scheme. Given that

$$\phi_n = \sum_{j=1}^{4}\phi_{bj} + \phi_p,$$

we can easily derive

$$\nabla\mu_{bj} = \nabla\mu_p = -\Gamma_1\nabla(\nabla^2\phi_n) + \Gamma_2\left(\frac{1}{N}\frac{1}{\phi_n+\varepsilon} + \frac{1}{1-\phi_n} - 2\chi\right)\nabla\phi_n, \quad j = 1,2,3,4$$

For simplicity, we denote

$$\mathcal{F}(\phi) = \Gamma_2\left(\frac{1}{N}\frac{1}{\overline{\phi}_n^{n+1}+\varepsilon} + \frac{1}{1-\overline{\phi}_n^{n+1}} - 2\chi\right)\nabla\phi - \Gamma_1\nabla\nabla^2\phi.$$

Then the numerical scheme for the transport equation of a biomass component is given by

$$\begin{cases} \frac{3\phi_{bj}^{n+1}-4\phi_{bj}^n+\phi_{bj}^{n-1}}{2\delta t} + \nabla\cdot(\overline{\phi}_{bj}^{n+1}\mathbf{v}^{n+1}) = \nabla\cdot\left[\Lambda\overline{\phi}_{bj}^{n+1}\mathcal{F}(\sum_{i=1}^4\phi_{bi}^{n+1}+\phi_p^{n+1})\right] + g_{bi}^{n+1}, \\ \frac{3\phi_p^{n+1}-4\phi_p^n+\phi_p^{n-1}}{2\delta t} + \nabla\cdot(\overline{\phi}_p^{n+1}\mathbf{v}^{n+1}) = \nabla\cdot\left[\Lambda\overline{\phi}_p^{n+1}\mathcal{F}(\sum_{i=1}^4\phi_{bi}^{n+1}+\phi_p^{n+1})\right] + g_p^{n+1}, \end{cases} \tag{3.1}$$

where $j = 1,2,3,4$. These five equations are solved simultaneously by a preconditioned BI-CG-stab routine, where the reactive terms are extrapolated to the $n+1$th time-step. The reactive terms are discretized

as follows:

$$
\begin{aligned}
g_{b1}^{n+1} &= \left[\frac{C_{b1}\overline{c}^{n+1}}{k_{b1}+\overline{c}^{n+1}}(1-\frac{\overline{\phi_b}^{n+1}}{\phi_{b,\max}})-r_1-\frac{r_{12}(\overline{A}^{n+1})^2}{\tau^2+(\overline{A}^{n+1})^2}-\frac{C_{d1}\overline{d}^{n+1}}{k_{d1}+\overline{d}^{n+1}}\right]\phi_{b1}^{n+1}+\frac{r_{21}\tau^2}{\tau^2+(\overline{A}^{n+1})^2}\overline{\phi_{b2}}^{n+1} \\
&\quad +\beta C_{b2}\frac{\overline{c}^{n+1}}{k_{b1}+\overline{c}^{n+1}}(1-\frac{\overline{\phi_b}^{n+1}}{\phi_{b,\max}})\overline{\phi_{b2}}^{n+1} \\
g_{b2}^{n+1} &= \left[\frac{(1-\beta)C_{b2}\overline{c}^{n+1}}{k_{b2}+\overline{c}^{n+1}}(1-\frac{\overline{\phi_b}^{n+1}}{\phi_{b,max}})-r_2-\frac{r_{21}\tau^2}{\tau^2+(\overline{A}^{n+1})^2}-\frac{C_{d2}\overline{d}^{n+1}}{k_{d2}+\overline{d}^{n+1}}\right]\phi_{b2}^{n+1}+\frac{r_{12}(\overline{A}^{n+1})^2}{\tau^2+(\overline{A}^{n+1})^2}\overline{\phi_{b1}}^{n+1}, \\
g_{b3}^{n+1} &= \left[\frac{C_{b3}\overline{c}^{n+1}}{k_{b3}+\overline{c}^{n+1}}(1-\frac{\overline{\phi_b}^{n+1}}{\phi_{b,max}})-r_3-\frac{C_{d3}\overline{d}^{n+1}}{k_{d3}+\overline{d}^{n+1}}\right]\phi_{b3}^{n+1}, \\
g_{b4}^{n+1} &= \sum_{i=1}^{3}\left[r_i+\frac{C_{di}\overline{d}^{n+1}}{k_{d3}+\overline{d}^{n+1}}\right]\overline{\phi}_{bi}^{n+1}-r_4\phi_{b4}^{n+1}, \\
g_{p}^{n+1} &= \sum_{i=1}^{3}\frac{C_{pi}\overline{c}^{n+1}}{k_{pi}+\overline{c}^{n+1}}\overline{\phi}_{bi}^{n+1}(1-\frac{\phi_p^{n+1}}{\phi_{p,\max}})+\alpha r_4\overline{\phi}_{b4}^{n+1}-r_p\phi_p^{n+1}-\frac{C_{dp}\overline{d}^{n+1}}{k_{dp}+\overline{d}^{n+1}}\phi_p^{n+1}.
\end{aligned}
\tag{3.2}
$$

At each time step, after the momentum equation and the transport equations for biomass components are solved, their updated data would be used to solve the transport equations of the functional molecules. These equations are also solved by a series of second order semi-implicit finite difference schemes, which are given below

$$
\begin{cases}
\frac{3\phi_s^{n+1}c^{n+1}-4\phi_s^n c^n+\phi_s^{n-1}c^{n-1}}{2\delta t}+\mathbf{v}^{n+1}\cdot\nabla(c^{n+1}\phi_s^{n+1})=\nabla\cdot(D_s^{n+1}\phi_s^{n+1}\nabla c^{n+1})+\overline{g}_c^{n+1}, \\
\frac{3\phi_s^{n+1}d^{n+1}-4\phi_s^n d^n+\phi_s^{n-1}d^{n-1}}{2\delta t}+\mathbf{v}^{n+1}\cdot\nabla(d^{n+1}\phi_s^{n+1})=\nabla\cdot(D_e^{n+1}\phi_s^{n+1}\nabla d^{n+1})+\overline{g}_d^{n+1}, \\
\frac{3\phi_s^{n+1}A^{n+1}-4\phi_s^n A^n+\phi_s^{n-1}A^{n-1}}{2\delta t}+\mathbf{v}^{n+1}\cdot\nabla(A^{n+1}\phi_s^{n+1})=\nabla\cdot(D_a^{n+1}\phi_s^{n+1}\nabla a^{n+1})+\overline{g}_a^{n+1}.
\end{cases}
\tag{3.3}
$$

where the discrete schemes for reactive terms are summarized below

$$
\begin{aligned}
g_a^{n+1} &= -r_a A^{n+1}+\left(\sum_{i=1}^{2}(r_{ai}+\frac{C_{ai}A^n}{k_{ai}+A^n})\phi_{bi}^{n+1}\right)(1-\frac{\overline{A}^{n+1}}{A_{\max}})-\frac{C_a\overline{d}^{n+1}}{k_{da}+\overline{d}^{n+1}}A^{n+1}, \\
g_c^{n+1} &= -\sum_{i=1}^{3}\frac{r_{bi}c^n}{k_{bi}+c^n}\phi_{bi}^{n+1}-\sum_{i=1}^{3}\frac{r_{pi}c^n}{k_{pi}+c^n}\phi_{bi}^{n+1}, \\
g_d^{n+1} &= -\frac{d^n}{k_d+d^n}(\sum_{i=1}^{4}r_{di}\phi_{bi}^{n+1}+r_{dp}\phi_p^{n+1})-r_d d^{n+1}.
\end{aligned}
\tag{3.4}
$$

These schemes are implemented in a CPU-GPU hybrid environment using CUDA to achieve parallelization and high performance computing. The implementation has been well-tested by reducing grid sizes in both time and space, and nearly second order convergence rate is observed.

4 Results and discussions

The hydrodynamic model of biofilms presented in section 2 is fairly general, which can be applied to study dynamic problems involving biofilms immersed in a viscous solvent. In this section, we apply it to investigate a few specific issues related to quorum sensing in biofilm formation, which include the effect of the threshold for quorum sensing induction and its impact to biofilm formation, and the effect of hydrodynamics on the distribution of autoinducers and its consequence to biofilm development.

As we alluded to earlier, the model contains many parameters, some of which need to be calibrated via experiments while others are either obtained from the literature or from our best guesses [**?**,**?**]. For instance, the wash-out-rates in the model, r_1, r_2, r_3, r_4, r_p, r_a and r_d are normally small; so, we set them into zero in the following discussion. For the monod constants (the k's), we choose a common value 3.5×10^{-4} as used in [**?**]. All the other parameters used in this paper are summarized in table **??**, unless mentioned otherwise.

4.1 Reactive kinetics in biofilms

We begin with the study on reactive kinetics in this model to elucidate bulk reactive kinetics for each component on two important mechanisms during biofilm development. By neglecting hydrodynamics, diffusive effects, and the drug effect in the model, as well as assuming nutrient is sufficiently supplied, we arrive at the governing equations for reactive kinetics in biofilms,

$$\begin{cases} \frac{d\phi_{b1}}{dt} &= \frac{(C_{b1}\phi_{b1}+\beta C_{b2}\phi_{b2})c}{k_{b1}+c}(1-\frac{\phi_b}{\phi_{b,\max}}) - \frac{r_{12}A^n}{\tau^n+A^n}\phi_{b1} + \frac{r_{21}\tau^n}{A^n+\tau^n}\phi_{b2}, \\ \frac{d\phi_{b2}}{dt} &= (1-\beta)\frac{C_{b2}c}{k_{b2}+c}\phi_{b2}(1-\frac{\phi_b}{\phi_{b,\max}}) + \frac{r_{12}A^n}{A^n+\tau^n}\phi_{b1} - \frac{r_{21}\tau^n}{A^n+\tau^n}\phi_{b2}, \\ \frac{d\phi_{b3}}{dt} &= \frac{C_{b3}c}{k_{b3}+c}\phi_{b3}(1-\frac{\phi_b}{\phi_{b,\max}}) - \frac{C_{d3}d}{k_{d3}+d}\phi_{b3}, \\ \frac{d\phi_p}{dt} &= \sum_{i=1}^{3}\frac{C_{pi}c}{k_{pi}+c}\phi_{bi}\left(1-\frac{\phi_p}{\phi_{p,\max}}\right), \\ \frac{dA}{dt} &= \left(\sum_{i=1}^{2}(r_{ai}+\frac{C_{ai}A}{k_{ai}+A})\phi_{bi}\right)\left(1-\frac{A}{A_{\max}}\right), \end{cases} \tag{4.1}$$

where $c = 1$ is used in the following discussion.

It is observed experimentally that biofilm formation can be affected dramatically by the threshold for quorum sensing induction. So, in the first case study, we focus on investigating the solution sensitivity on the threshold parameter τ. For simplicity and without loss of generality, we conduct a simulation with only quorum sensing bacteria in the system, where we simulate biofilm formation with a few selected quorum sensing threshold values. One set of simulation results is depicted in Figure **??**. It shows that the lower the threshold value is, the quicker quorum sensing induction can take place so that quorum sensing up-regulated bacteria can begin to grow, eventually its population will catch up or even overtake that of the quorum sensing down-regulated bacteria. As more QS up-regulated bacteria become available, the amount of EPS production increases, leading to the formation of robust biofilms. For any fixed threshold value, a steady state exists for the bacterial populations as well as the EPS capacity after sometime in this model. When biofilm development reaches a steady state, the ratio of the concentration of the up-regulated bacteria to that of the down-regulated bacteria decreases drastically as the threshold value increases. Besides, the transient exponential growth phase for bacteria is captured and the transition between these two bacterial phenotypes is shown at the moment when the density of the QS molecules reaches the threshold. This phenomenon has been observed in many experiments and is now confirmed by this simplified bulk kinetic model. We remark that, for both the bacterial growth and the EPS production, we implemented logistic growth modes in the model so that the steady state is limited to an environmentally sustainable level.

Secondly, we study the case of competition between QS bacteria and non QS bacteria in a biofilm system with respect to the growth rate of the QS down-regulated bacteria C_{b1}. There are many parameters in this model, our extensive parameter studies show that the biofilm dynamics is sensitive to the growth rate C_{b1} of the QS down-regulated bacteria. Suppose that we have 10% non-quorum sensing bacteria initially populated in the system. We simulate biofilm formation with respect to the growth rate of QS down-regulated bacteria. The result is depicted in Figure **??**.

If the growth rate is high, the total bacterial volume fraction is not affected much over time even when it reaches a steady state, and, in the meantime, non-quorum sensing bacteria are kept in a low volume fraction. In this case, the biofilm formation with an exponential growth and EPS production are observed in transient. However, when the growth rate is low, the total biomass reaches a steady state at a slower pace, which is primarily controlled by non-quorum sensing bacteria and eventually the non QS regulated bacteria take control over the whole colony should the initial volume fraction of the non QS regulated bacteria be high. The result shown in Figure **??** is with respect to four selected values of growth rate C_{b1} in 6 days, in which the volume fraction of non-QS bacteria at the lowest growth rate $C_{b1} = 8 \times 10^{-5}$ is approximately 10 times higher than that of QS bacteria at the end of the 6th day, whereas the volume fraction of non-QS bacteria barely changes at the highest growth rate of $C_{b1} = 8 \times 10^{-4}$. This result suggests that quorum sensing in biofilms may not always be a beneficial mechanism for growth when there is a large amount of non-QS regulated bacteria present, as it might be taken advantage of by other phenotypes or even enemies.

A complete parameter study of this reactive kinetics model perhaps would warrant another paper, which will not be pursued further in this paper. We next turn to the full hydrodynamic model to examine two quorum sensing related mechanisms that affect the heterogeneous biofilm formation.

4.2 Biofilm development coordinated by quorum sensing

Biofilm formation is a process, where bacteria aggregate in space and secrete glue-like exopopolysacharrides or extra cellular polymeric substances (EPS) to form a bio-network around the bacteria, which creates a barrier between the bacteria and the surrounding media. It has been observed that quorum sensing controls biofilm formation in vibrio cholerae [**?**] by regulating transcription of genes involved in expopolysacharride production (i.e., EPS production). Other observations on quorum sensing regulated EPS production can also be found in Pseudomonas aeruginos [**?**], sinorhizobium meliloti [**?**], as well as in some other bacterial systems [**?**].

Since there has not been a consensus on what is the role of quorum sensing during biofilm formation, we will focus on simulating the mechanism of quorum sensing regulated EPS production using the model in a heterogeneous biofilm colony and studying benefits and drawbacks of QS regulation during biofilm formation in the following.

4.2.1 Biofilm development coordinated by quorum sensing

For simplicity, we suppress the non-QS regulated bacteria in the first case study, i.e., we consider a model biofilm system where only QS-regulated bacteria are present initially. We set the initial value of ϕ_{b3} (the volume faction of non QS regulated bacteria) to zero and assume that the dead bacteria are all dissolved in the solvent instantly. This way, we can highlight how quorum sensing induction takes place and how the biofilm developmental dynamics can be coordinated by the density of the QS molecules. We aim our numerical simulations at heterogeneous biofilm formation in an aqueous environment where laminar flows can be present. The scenarios include a culture petri dish filled with water or a long water channel where nutrient is constantly supplied through the solution surface.

Figure **??** depicts a result from the simulation, where solutions are shown at $t = 0$ and $t = 300$, respectively. In this simulation, some QS down-regulated bacteria (QS^-) are assumed to be attached to the substrate surface initially and the bacterial cell reproduction ensues as soon as the simulation begins. As a result, the QS molecule is produced and its concentration keeps growing. Once the density of the quorum sensing molecules exceeds the threshold value τ, QS^- start to bind with QS molecules and undergo a phenotypic change into quorum sensing up-regulated bacteria QS^+, for which the gene expression for reproduction for both cells and EPS is switched on. The biofilm colony starts growing exponentially by reproducing bacteria as well as secreting EPS, necessary extracellular RNA and enzymes. With more QS

molecules produced, QS^+ eventually outgrow QS^- and populate the bulk part of the biofilm colony. In the result, we observe that QS^- tend to be seen near the surface of the biofilm colony. The 3D result for volume fractions of total bacteria, QS downregulated and QS upregulated bacteria, EPS and the total biomass are depicted in Figure **??**.

The model predicts that QS-regulated EPS production contributes to the formation of heterogeneous biofilm structures. As shown in Figure **??**(b), the distribution of live bacteria is highly heterogenous, QS^- are mainly located at the surface of the biofilm, where they can access nutrients more easily, and QS^+ are located more in the bulk of the biofilm colony. This mushroom shaped biofilm morphology qualitatively agrees with the published result on the morphological pattern in Pseudomonas aeruginosa biofilms [**?**].

In order to show details of this process, plots of three slices at $x = 0.16, y = 0.04, z = 0.16$ for different biofilm components are shown in Figure **??** and **??**, respectively. In Figure **??**(c), where the average velocity is small, the distribution of the QS molecules (AHLs) is dominated mainly by spatial diffusion. Meanwhile, we observe that QS molecules are mainly distributed within the biofilm colony although small amount can diffuse into the solvent, illustrated by a three-slice plot in Figure **??**(b). The biomass flux at $z = 0.5$ is plotted in Figure **??**(d). It shows that it is mainly distributed at the top surface between the biomass the surrounding solvent, where there are more nutrients available at the surface than in other places so that the biomass tends to grow the fastest in these places. A pressure profile is also plotted in a slice, which shows that a high pressure is observed in the interior while a low one is present near the surface. This numerical simulation explains the growth process of the biofilm due to QS regulated bacteria and QS-regulated EPS production. Of course, the biomass can't grow without a sufficient nutrient supply. But, in this case study, we assume its role is secondary.

4.2.2 Benefits and drawbacks of quorum sensing regulation

Now that biofilm formation is regulated by quorum sensing, a straight forward question is if this quorum sensing mechanism is always beneficial? Experimental findings seem to suggest the answer is "it depends." As the production of QS molecules is energetically costly, bacteria probably would switch on the quorum sensing mechanism to start producing QS molecules whenever they are in the "right time" and "right place." In this subsection, we would like to further investigate the so called 'right time' and 'right place' such that the QS regulation for EPS production can be in favor of the biofilm development.

Through numerical simulations, we find that the model predicts that quorum sensing regulation is not beneficial to biofilm formation in a short time frame when competing with invading strains of bacteria. In other words, given a highly reproductive invasion strain (like non-QS regulated bacteria), QS-regulated bacteria can lose the competition such that the non-QS regulated bacteria can take over and eventually populate the whole biofilm colony, which is mentioned in the case study of bulk reactive kinetics.

To illustrate the point, let's consider a biofilm system with three different phenotypes of QS regulated bacteria: QS^-, QS^+ and non-QS. In this system, we suppose that non-QS regulated bacteria have the same reproductive rate as that of QS^-, but do not bind QS molecules and convert themselves into QS^+. We conduct a numerical simulation, taking into account all these three phenotypes to study the detail of how the interaction between these bacteria can affect biofilm development via different self-production and EPS production rates. In this simulation, initially some QS^- and non-QS regulated bacteria with the same volume fraction are assumed to be attached to the substrate surface. We assume $C_{b1} = C_{b3}$ and the growth rate for QS up-regulated bacteria C_{b2} is smaller. A 3D view of the biofilm growth process predicted by our 3D simulations is displayed in Figure **??**. As shown in Figure **??**(b), non-QS regulated bacteria outgrow the QS regulated bacteria and take over the whole biofilm colony eventually. This is because the QS regulated bacteria undergo mutual conversion which slows down the reproduction of QS^+ bacteria as well as QS^-. The total volume fraction for each type of bacteria is plotted in **??**(c), where non-QS bacteria grow exponentially, while QS regulated bacteria grows only slightly. Since non-QS regulated bacteria have

a higher effective reproduction rate than those of QS regulated ones combined effectively, non-QS regulated bacteria eventually grow faster to gain more access to nutrient. Hence, the density of non-QS regulated bacteria can eventually take over that of QS regulated bacteria in a majority part of the biofilm colony due exclusively to the quorum sensing effect.

In addition, our simulations also show that quorum sensing regulation is not beneficial to biofilm development in a short time, especially, in terms of gaining biomass. To expose the feature, we conduct another numerical simulation, where the quorum sensing mechanism is switched off by setting $r_{21} = r_{12} = 0$ while the other model parameters are retained as in the previous numerical experiment. It is shown in Figure **??** that the volume fraction of the total live bacteria without quorum-sensing regulation is higher than that with quorum sensing regulation switched on. However, the total biomass in the system without QS regulation, including EPS and bacteria, is much less than that with QS regulation. This indicates that QS regulation is not a way to reproduce bacteria, but rather a way to increase the amount of EPS so as to expand biofilm colony, especially, in a short time frame. The result agrees qualitatively with the experimental observation reported in [**?**].

In the long term however, our numerical studies show that QS regulation is of benefit to stabilizing biofilm colony and settling on the host, as well as protecting bacteria from environmental stress. Given the protective nature of EPS, the biofilm colony can become more stable and resistant to external stress while more EPS is produced. EPS can protect bacteria from being attacked by antimicrobial agents or immune systems of the host. To illustrate the beneficial effect of quorum sensing, we conduct a numerical experiment with the drug/disinfectant effect included. The result is shown in Figure **??**. In this simulation (see Figure **??**(f)), non-QS regulated bacteria are killed dramatically while QS regulated bacteria are killed in a much slower pace. Our model and simulation confirm that EPS acts as a barrier to protect bacteria from being attacked. In Figure **??**(a) and Figure **??**(b), we notice that bacteria staying within the environment filled with EPS lives longer under antimicrobial drug treatment. In Figure **??**(e), we see that drug penetrates less in the place where there exists more EPS than in the place with less EPS. This numerical result agrees qualitatively with the claim made in [**?**], that biofilms can benefit from quorum sensing induced EPS production if bacteria cells have the objective of acquiring a thick, protective layer of EPS. This may also explain why antimicrobial drugs are more effective for young biofilms; when biofilms have grown for weeks, the effect of antimicrobial drugs drops significantly. When the biofilm is young, there exists less EPS surrounding it; when the biofilm is "old", however, the QS induced EPS has already accumulated around bacterial cells so that they can prevent drugs from penetrating deeper into the biofilm. This agrees qualitatively well with the observation reported in [**?**] that biofilms at an earlier age is more susceptible to antimicrobial treatment than those in an older age.

We have used two numerical experiments to elucidate the role of quorum sensing in the development of biofilms. Benefits or detriments of quorum sensing for biofilms depend on many factors, for instance, the age of biofilms, if antimicrobial treatment is involved, growing the biofilm or eradicating the biofilm, etc. Quorum sensing regulation tends to slow down the production of bacteria while in the meantime promote the production of EPS, which is beneficial to the development of a robust biofilm in a long run but detrimental to the biofilm formation in a short time. Nevertheless, quorum sensing is an important mechanism for biofilm development. An ultimate determination of its role can only be rendered in connection with the specific situation where biofilm's issues are concerned. Next, we turn to discussing the interaction between hydrodynamics and quorum sensing during the development of biofilms in an aqueous environment.

4.3 Interaction between biofilm hydrodynamics and quorum sensing

4.3.1 Quorum sensing in an aqueous environment

Many biofilms grow in an aqueous environment ranging from laminar flows, such as river bank or pipes, to quiescent aqueous environment. It is observed that a flow environment can impact on the QS induction during biofilm formation [**?**, **?**]. In return, the hydrodynamically altered QS induction can affect biofilm structures and functions. However, there is little known on the detail of how hydrodynamic factors actually affect QS induction. Here, we use the hydrodynamic model along with the developed numerical simulating tool to investigate some of the effects in details. Again for simplicity, we consider the case there are only QS regulated bacteria in the biofilm system, i.e. QS^- bacteria and QS^+ bacteria, as we are interested in how quorum sensing induction is affected by hydrodynamic factors. The boundary conditions used in the simulation are set up to mimic biofilm development in a flow cell, where the fluid (solvent) flows through continuously.

Firstly, we conduct a numerical simulation of the biofilm system subject to a varying inlet fluid velocity and focus on biofilm formation under hydrodynamic shear. The result is shown in Figure **??**. Initially, some QS^- bacteria are attached at the center of the flow cell. Solvent containing nutrient keeps flowing through the flow-cell while the bacteria grow into a biofilm colony. As shown in Figure **??**(c), a higher hydrodynamic shear can actually dilute the concentration of QS molecules, which leads to a delay in QS induction. With the diluted QS molecular concentration, the biofilm in the flow cell with a higher inlet velocity has a less volume fraction of QS^+ bacteria. Note however that a biofilm with a higher inlet velocity results in a higher volume fraction of the total bacteria. This is because the nutrient supply at a higher inlet velocity can bring in more nutrient and thus facilitates the growth of all bacteria. A robust biofilm colony needs not only the growth of bacteria, but also the build-up of EPS. Since the EPS growth by QS^+ is more than that by QS^-, a reduced QS^+ production leads to the reduced EPS production in the biofilm. Even though the total bacteria is not reduced, the EPS production is reduced by the higher in-let velocity. 2D slices (at $z = 0.5$) of QS molecules and QS^+ bacteria at time $t = 25$ are shown in Figure **??**. This numerical experiment demonstrates that the maximum concentration of Qs molecules and the volume fraction of QS^+ are higher in the flow cell when subject to a slower inlet speed and the scenario is reversed when the inlet speed is higher.

This study suggests that hydrodynamics can have a strong influence on quorum sensing. A higher inlet flow dilutes the concentration of the QS signaling molecules, which then requires a higher cell density and delayed time for quorum sensing induction to take place. This means that QS may not be fully operational at high flow rates and thus indicates that the role of QS in biofilm formation can be compromised in a flow environment.

We note that how quickly QS molecules are produced, how quickly the QS molecules diffuse away from the biofilms and the critical concentration of QS molecules are three main factors affecting biofilm formation. When taking into account of the effect of nutrient, especially, when the growth due to nutrient dominates, the diffusion rate and consumption rate of nutrient can be essential for the biofilm growth as well. We hope the theoretical result can be quantitatively confirmed experimentally in the near future.

4.3.2 Effect of nutrient to the interaction between hydrodynamics and quorum sensing

Compared with a quiescent aqueous environment, the big difference of biofilms developed in a flow cell is their structural heterogeneity in the flow field, due to the hydrodynamic stress and inhomogeneous nutrient distribution. Mass transfer in the fluid mixture can be affected by hydrodynamics of the bulk fluid and the morphology of the biofilm colony. Under a flow environment, one natural question to ask is which part of biofilms, especially bacteria living upstream or downstream, is benefited from quorum sensing regulation more. For this, we conduct a numerical simulation with a distribution of biofilm colonies in the flow channel.

Our numerical simulations suggest that biofilms upstream can induce downstream biofilms to quorum-sense under the flow if they are close enough spatially, which is in agreement with the result in [**?**]. In Figure **??**, we demonstrate that quorum sensing takes place at downstream firstly, that's quorum sensing induction takes place at the last four colonies instead of the first one located upstream. It also shows that the downstream region tends to have a higher concentration of QS molecules than at the location upstream in Figure **??**(g), which we believe is an amplification of the convection and diffusion effect of Qs molecules .

However, we note that this may not be always true, especially when nutrient supply is strong. A comparison with different nutrient supply rates is shown in Figure **??**. We observe that, at an early stage, bacteria downstream can be benefitted since QS molecules are more diluted upstream (see Figure **??**(c)). QS induction is more effective downstream since there exist more QS^+ bacteria there (see Figure **??**(b)). But when time passes by and the nutrient supply is kept at a sufficiently high level, it seems that quorum sensing induction benefits from a higher flow velocity since it sustains a sufficient nutrient supply that facilitates the growth of all bacteria as well the production of QS molecules. As a result, the overall production of QS molecules upstream overcomes the dilution of QS molecules such that both the concentration of QS molecules and the volume fraction of bacteria are higher upstream. In Figure **??**(e), we can see there are more QS^+ bacteria upstream than downstream in this case. Figure **??**(h) depicts the EPS production in the flow cell, which can also be tied to the excessive accessibility to nutrient.

4.3.3 Biofilm morphology under a strong shear flow

In previous discussions, we focus on interactions between hydrodynamics and quorum sensing induction under the assumption that the biofilm grows under weak flow fields. When the flow is strong, however, biofilms can undergo significant morphological changes and most of the biofilms can perhaps be flushed out of the flow cell. To better illustrate the hydrodynamic impact on biofilm structures and QS induction in strong flows, we conduct a numerical simulation where a grown biofilm colony is subject to a string shear flow in a flow cell. Here, we put two biofilm colonies in a $4\times1\times1$ domain, representing a flow cell with inlet and outlet boundaries in the x direction. The initial biofilm profile is shown in Figure **??**(a). From **??**(b), we notice that the biofilm undergoes a significant morphological change under the shear. The colonies are tilted under the shear. The one near the inlet boundary is about to detach from the bottom in Figure **??**(d). In addition, a fast flow can dilute QS molecules as they are readily convected out of the flow cell shown in Figure **??**(c) and (e).

The advantage of our full 3D hydrodynamic model, compared with those in lower dimension, as well as reaction-diffusion models is its capability to resolve the flow detail and hydrodynamically as well as rheologically significant quantities such as the normal stress differences and shear stress components. Here, these stress components related to the simulation above are depicted in Figure **??**. In Figure **??**, we only show the sign of $\phi_n\tau$, the effective stress for the biomass component, where we use red to represent negative and blue positive values of the stress. It is seen through Figure **??**(e) that the first normal stress difference is positive at the top of the biofilm region while negative around the neck facing the inlet boundary, which means that the normal stress τ_{xx} is larger than τ_{yy} at the top of the biofilm mechanically providing a drag force along the x direction. This is confirmed by Figure **??**(c), where the top of the biofilm is stretched towards the x direction. In addition, through Figure **??**(D), the second normal stress difference is positive at the neck facing the inlet boundary, where τ_{yy} is larger than τ_{zz} resulting in a stretching of the biofilm colony toward the y direction. This is supported by the fact that the neck becomes thinner due to this stretch, shown in Figure **??**(c). In addition, the other three components of shear stress tensor are also depicted in Figure **??**(f-g). On a y plane, i.e. the plane $y = a$ $(0 < a < 1)$, we see the shear stress τ_{xy} is positive, which forces the biofilm towards the x direction (shown in the comparison of Figure **??**(b) and (c).) The effect of τ_{xz} and τ_{yz} can also be observed on a z-plane, i.e. $z = a$ $(0 < a < 1)$, shown in Figure **??**(g), where τ_{xz} provides a shear stress towards the x direction on the top of the biofilm mushroom shaped colony and τ_{yz} provides a

shear stress towards the y direction on the top of the mushroom.

5 Conclusion

In this paper, a hydrodynamic phase field model for biofilms is developed to study biofilm development coordinated by quorum sensing, extending our previous biofilm models for binary mixture [**?**]. By identifying appropriate bacterial types based on their function in quorum sensing in the biofilm and proposing the corresponding reactive kinetics, we are able to describe several bulk phenomena related to quorum sensing induction using the new model. We then develop a numerical scheme to solve the governing system of equations in the model and implement it in 3D space and time. Then we are able to simulate and predict heterogeneous spacial-temporal structures of a biofilm in terms of its volume fractions for each bacterial component, EPS and solvent. The simulation tool is put in use to study a set of selected mechanisms in quorum sensing regulated biofilm development.

Our numerical simulations indicate that QS-regulated EPS production acts as a means of competition for both space and nutrient since higher EPS production rate can help to expand biofilm colonies spatially without reaching a higher local density. In addition, numerical simulations confirm the hypothesis that QS regulated EPS production acts as a means for promoting biofilm development as well as protecting biofilms from the environment stress, such as antimicrobial treatment and hydrodynamical stress etc. However, quorum sensing regulation is not universally beneficial to biofilm development in all situations evidenced by what we have shown that an invasion strain of bacteria with a high production rate can out-grow QS regulated bacteria, as QS induction can retard the proliferation of bacteria, thereby the development of biofilms, in a short time window.

By simulating biofilms in a flow cell, hydrodynamic effects on quorum sensing are investigated in details. The model can capture the competition between the dynamic diluting effect and the nutrient supply for QS induction well. Our simulations predict that downstream bacteria can be benefited from higher in flow speed to initiate QS induction earlier. However, the model also shows that this only takes place in a short time window, where the nutrient supply is weak. When the nutrient supply is strong, it is a competition between the hydrodynamic dilution of QS molecules and the nutrient supply for the production of QS molecules that ultimately determines which part of biofilms in a flow cell would benefit more.

This 3D hydrodynamic model provides a powerful predicative tool to allow us to investigate quorum sensing regulated biofilm development and some factors that correlate with quorum sensing and their interaction with hydrodynamics. It is a robust, hands-on tool for analyzing the mechanism of quorum sensing in biofilm dynamics. In addition to the phenomena that we numerically confirmed, we hope results predicted here can be verified experimentally in the near future. In our subsequent research, other quorum sensing regulated factors such as virulence, resistance to antimicrobial agents will be investigated.

Acknowledgement

Qi Wang is partially supported by AFOSR, NIH and NSF through awards FA9550-12-1-0178, DMS-1200487, and 2R01GM078994-05A1.

References

[1] Erik Alpkvist, Cristian Picioreanu, Mark C. M. van Loosdrecht, and Anders Heyden. Three-dimensional biofilm model with individual cells and continuum eps matrix. *Biotechnology and Bioengineering*, 94(5):961–979, August 2006.

[2] Swati Choudhary and Claudia Schmidt-Dannert. Applications of quorum sensing in biotechnology. *Applied Microbiology and Biotechnology*, 86:1267–1279, 2010.

[3] N.G. Cogan. Effects of persister formation on bacterial response to dosing. *Journal of Theoretical Biology*, 238:694–703, February 2006.

[4] M. Fauvart, P. Phillips, D. Bachaspatimayum, N. Verstraeten, J. Fransaer, J. Michiels, and J. Vermant. Surface tension gradient control of bacterial swarming in colonies of pseudomonas aeruginosa. *Soft Matter*, 8:70–76, 2012.

[5] Mallory R Frederick, Christina Kuttler, Burkhard A Hense, and Hermann J Eberl. A mathematical model of quorum sensing regulated eps production in biofilm communities. *Theoretical Biology and Medical Modelling*, 2011.

[6] MR Frederick, C Kuttler, BA Hense, J Muller, and HJ Eberl. A mathematical model of quorum sensing in patchy biofilm communities with slow background flow. *Canadian Applied Mathematics Quarterly*, 18(3):267–298, 2010.

[7] Cristina Garcia-Aljaro, Silvia Melado-Rovira, Debra L Milton, and Anicet R Blanch. Quorum-sensing regulates biofilm formation in virio schophthalmi. *BMC Microbiology*, 12:287, 2012.

[8] J. L. Guermond, P. Minev, and Jie Shen. An overview of projection methods for incompressible flows. *Computer Methods in Applied Mechanics and Engineering*, 195:6011–6045, 2006.

[9] Brain K. Hammer and Bonnie L. Bassler. Quorum sensing controls biofilm formation in vibrio cholerae. *Molecular Microbiology*, 50(1):101–114, 2003.

[10] Douglas M. Heithoff and Michael J. Mahan. Vibrio cholerae biofilms: stuck between a rock and a hard place. *Journal of Bacteriology*, 186(15):4835–4837, 2004.

[11] Morten Hentzer and Michael Givskov. Pharmacological inhibition of quorum sensing for the treatment of chronic bacterial infections. *The Journal of Clinical Investigation*, 112(9):1300–1307, 11 2003.

[12] R. Hinson and W. Kocher. Model for effective diffusivities in aerobic biofilms. *Journal of Environmental Engineering*, 122(11):1023–1030, 1996.

[13] Mary Jo Kirisits, Jeffrey J. Margolis, Boloroo L. Purevdorj-Gage, Benjamin Vaughan, David L. Chopp, Paul Stoodley, and Matthew R. Parsek. Influence of the hydrodynamic environment on quorum sensing in pseudomonas aeruginosa biofilms. *Journal of Bacteriology*, 189, November 2007.

[14] Isaac Klapper and Jack Dockery. Mathematical description of microbial biofilms. *SIAM Review*, 52(2):221–265, may 2010.

[15] Kim Lewis. Persister cells. *Annual Review of Microbiology*, 64(1):357–372, 2010.

[16] Brandon Lindley, Qi Wang, and Tianyu Zhang. A multicomponent model for biofilm-drug interaction. *Discrete and Continuous Dynamical Systems Series B*, 15:417–456, March 2011.

[17] Melanine M. Marketon, Sarah A. Glenn, Anatol Eberhard, and Juan E. Gonzalez. Quorum sensing controls exopolysaccharide production in sinorhizobium melioti. *Journal of Bacteriology*, 185(1):325–331, January 2003.

[18] Melissa B. Miller and Bonnie L. Bassler. Quorum sensing in bacteria. *Annual Review of Microbiology*, 55:165–199, 2001.

[19] Carey D. Nadell, Joao B. Xavier, Simon A. Levin, and Kevin R. Foster. The evolution of quorum sensing in bacterial biofilms. *PLoS Biology*, 6(1):0171–0179, 2008.

[20] K. Nealson, T. Platt, and J.W. Hastings. The cellular control of the synthesis and activity of the bacterial luminescent system. *Journal of Bacteriology*, 104(1):313–322, 1970.

[21] Matthew R. Parsek and Tim Tolker-Nielsen. Pattern formation in pseudomonas aeruginosa biofilms. *Current Opinion in Biotechnology*, 11:560–566, 2008.

[22] Cristian Picioreanu, Mark C. M. van Loosdrecht, and Joseph J. Heijnen. Mathematical modeling of biofilm structure with a hybrid differential discrete cellular automaton approach. *Biotechnology and Bioengineering*, 58(1):101–116, April 1998.

[23] Roman Popat, Shanika A. Crusz, Marco Messina, Paul Williams, Stuart A. West, and Stephen P. Diggle. Quorum-sensing and cheating in bacterial biofilms. *Proceedings of the Royal Society B: Biological Sciences*, 279(1748):4765–4771, 2012.

[24] Beatriz Quinones, Glenn Dulla, and Steven E. Lindow. Quorum sensing regulates exopolysaccharide production, motility, and virulence in pseudomonas syringae. *Molecular Plant Microbe Interactions*, 18(7):682–693, 2005.

[25] Mark E. Roberts and Philip S. Stewart. Modeling protection from antimicrobial agents in biofilms through the formation of persister cells. *Microbiology*, 151:75–80, 2005.

[26] Yumiko Sakuragi and Roberto Kolter. Quorum-sensing regulation of the biofilm matrix genes (pel) of pseudomonas aeruginosa. *Journal of Bacteriology*, 189(14):5383–5386, July 2007.

[27] Jose A. Sanclement, Paul Webster, John Thomas, and Hassan H. Ramadan. Bacterial biofilms in surgical specimens of patients with crhonic rhinosinusitis. *Laryngoscope*, 115(4):578–582, April 2005.

[28] Jeffrey W. Schertzer, Megan L. Boulette, and Marvin Whiteley. More than a signal: non-signaling properties of quorum sensing molecules. *Trends in Microbiology*, 17:189–195, May 2009.

[29] Ya Shen and Markus Haapasalo. Antimicrobial efficacy of chlorhexidine against bacteria in biofilms at different stages of development. *Basic Research-Biology*, 2011.

[30] Ya Shen, Jia Zhao, Cesar de la Fuentz-Nunez, Zhejun Wang, Robert E. W. Hancock, and Qi Wang. Development and experimental validation of a model for oral multispecies biofilm recovery after chlorhexidine treatment. *submitted to PLoS ONE*, 2013.

[31] Stefanie Sonner, Messoud A. Efendiev, and Hermann J. Eberl. On the well-posedness of a mathematical model of quorum-sensing in patchy biofilm communities. *Mathematical Methods in the Applied Sciences*, 34:1667–1684, 2011.

[32] P S Stewart. Theoretical aspects of antibiotic diffusion into microbial biofilms. *Antimicrobial Agents and Chemotherapy*, 40(11):2517–22, 1996.

[33] Philip S. Stewart. Diffusion in biofilms. *Journal of Bacteriology*, 185(5):1485–1491, Mar 2003.

[34] Benjamin Vaughan, Bryan Smith, and David Chopp. The influence of fluid flow on modeling quorum sensing in bacterial biofilms. *Bulletin of Mathematical Biology*, 72(5):1143–1165, 2010.

[35] Cuong Vuong, Christiane Gerke, Greg A. Somerville, Elizabeth R. Fischer, and Michael Otto. Quorum-sensing control of biofilm factors in staphylococcus epidermidis. *Journal of Infectious Diseases*, 188(5):706–718, 2003.

[36] Qi Wang and Tianyu Zhang. Review of mathematical models for biofilms. *Solid State Communications*, 150(21):1009–1022, June 2010.

[37] John P. Ward and John R. King. Thin-film modelling of biofilm growth and quorum sensing. *Journal of Engineering Mathematics*, 73(1):71–92, 2012.

[38] John P. Ward, John R. King, A. J. Koerber, P. Williams, J. M. Croft, and R. E. Sockett. Mathematical modelling of quorum sensing in bacteria. *Mathematical Medicine and Biology*, 18(3):263–292, 2001.

[39] Christopher M. Waters and Bonnie L. Basseler. Quorum sensing: Cell-to-cell communication in bacteria. *Annual Review of Cell and Developmental Biology*, 21(1):319–346, 2005.

[40] Neil A. Whitehead, Anne M.L. Barnard, Holly Slater, Natalie J.L. Simpson, and George P.C. Salmond. Quorum sensing in gram-negative bacteria. *FEMS Microbiology Reviews*, 25:365–404, 2001.

[41] Joao B. Xavier and Kevin R. Foster. Cooperation and conflict in microbial biofilms. *PNAS*, 104(3):876–881, January 2007.

[42] Tianyu Zhang, Nick G. Cogan, and Qi Wang. Phase-field models for biofilms i. theory and simulations. *SIAM Journal of Applied Mathematics*, 69:641–669, 2008.

[43] Tianyu Zhang, Nick G. Cogan, and Qi Wang. Phase-field models for biofilms ii. 2-d numerical simulations of biofilm-flow interaction. *Communication in Computational Physics*, 4(1):72–101, July 2008.

Table 1: Parameters and their Values. Parameters with references for their order-of-magnitude are marked, otherwise they are fitted by our previous work and experience.

Symbol	Description	value	Unit	Source
h	Characteristic length scale	1×10^{-3}	m	[?]
t_0	Characteristic time scale	1000	s	[?]
L_x, L_y, L_z	size of computational domain	$1 - 2 \times 10^{-3}$	m	[?]
c_0, d_0, a_0	Characteristic Nutrient concentration	8.24×10^{-3}	$kg\, m^{-3}$	[?]
T	Absolute Temperature	303	K	[?]
k_B	Boltzmann constant	1.38×10^{-23}	$m^2 kg s^{-2} K^{-1}$	[?]
γ_1	Distortional energy coefficient	8×10^6	m^{-1}	[?]
γ_2	Mixing free energy coefficient	3×10^{17}	m^{-3}	[?]
χ	Flory Huggins parameter	0.55		[?]
λ	Mobility parameter	1×10^{-9}	$kg^{-1} m^3 s$	
N	Generalized polymerization	1×10^3		[?]
ρ_n	Network density	1×10^3	$kg\, m^{-3}$	[?]
ρ_s	Solvent density	1×10^3	$kg\, m^{-3}$	[?]
η_p, η_b	Dynamic viscosity of biomass	10	$kg\, m^{-1} s^{-1}$	
η_s	Dynamic viscosity of solvent	1.002×10^{-3}	$kg\, m^{-1} s^{-1}$	[?]
D_{c0}	Nutrient diffusion coefficient	2.3×10^{-9}	$m^{-2} s^{-1}$	[?]
D_{a0}	AHL diffusion coefficient	2.3×10^{-10}	$m^{-2} s^{-1}$	[?]
D_{d0}	Antimicrobial diffusion coefficient	2.3×10^{-9}	$m^{-2} s^{-1}$	[?]
C_{b1}	bacteria growth rate for QS^-	4.0×10^{-4}	s^{-1}	[?]
C_{b2}	bacteria growth rate for QS^+	1.0×10^{-4}	s^{-1}	[?]
C_{b3}	bacteria growth rate for non-QS	4.0×10^{-4}	s^{-1}	[?]
C_{d1}, C_{d2}, C_{d3}	death rate due to drug	4.0×10^{-2}	s^{-1}	[?]
r_{12}, r_{21}	transfer rate between ϕ_{b1} and ϕ_{b2}	4×10^{-3}	s^{-1}	
C_{p1}, C_{p3}	Growth rate of ϕ_p due to ϕ_{b1} and ϕ_{b3}	1×10^{-7}	s^{-1}	
C_{p2}	Growth rate of ϕ_p due to ϕ_{b2}	4×10^{-4}	s^{-1}	
$r_{a1}, r_{a2}, C_{a1}, C_{a2}$	growth rate of AHL	4×10^{-5}	s^{-1}	
$r_{di}, r_{dp}, r_{bi}, r_{pi}, i = 1, 2, 3$	drug and nutrient consumption rate	4×10^{-2}	s^{-1}	
D_{pr}	Hinson model constant	0.02		[?]
$\phi_{b,max}$	carrying capacity for bacteria	0.15		
$\phi_{p,\max}$	carrying capacity for EPS	0.2		
τ	threshold of quorum sensing	0.5		
β	bacteria growth rate ratio	1.0		

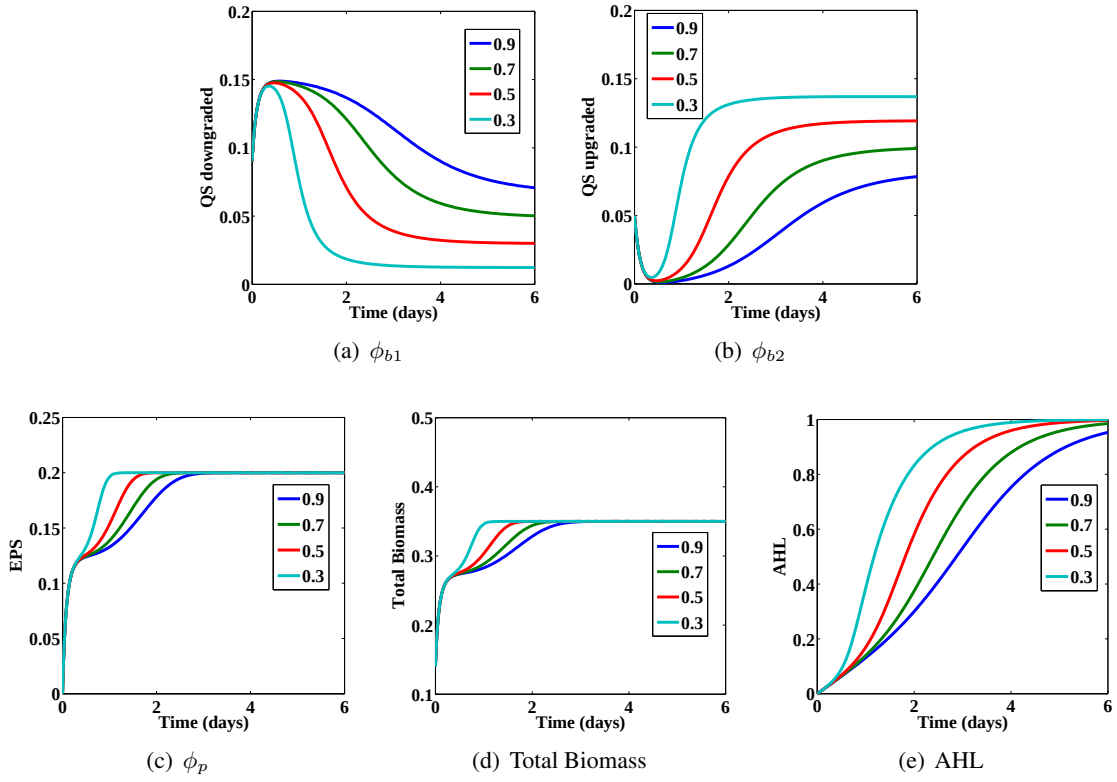

(a) ϕ_{b1} (b) ϕ_{b2}

(c) ϕ_p (d) Total Biomass (e) AHL

Figure 2: Biofilm development with only QS bacteria in the biofilm system. This simulation demonstrates the effect of QS threshold value τ for quorum sensing induction on biofilm development. The QS threshold values used are $\tau = 0.3, 0.5, 0.7, 0.9$, respectively, and $r_{12} = r_{21} = 10^{-4}, \beta = 0$. The volume fraction of QS down-regulated bacteria, QS up-regulated bacteria, EPS and total bacteria, respectively, and AHL concentration are shown as functions of time in the subfigures. (a) The volume fraction of QS down-regulated bacteria. (b) The volume fraction of QS up-regulated bacteria. (c) The volume fraction of EPS. (d) The volume fraction of the total bacteria. (e) The concentration of autoinducers/QS molecules: AHL. The simulation shows that the smaller the threshold value τ is, the sooner QS induction takes place. The sooner QS induction takes place, the faster QS up-regulated bacteria can grow, leading to steady states in EPS production as well as the total biomass sooner. The production of QS molecules decreases as the threshold value increases.

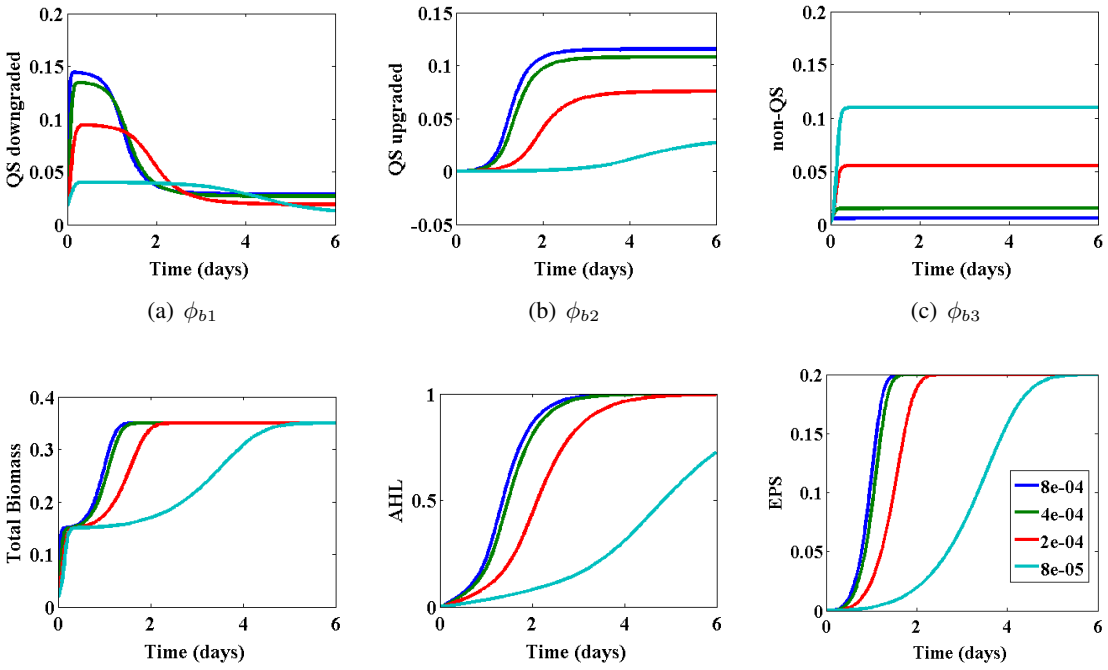

(a) ϕ_{b1} (b) ϕ_{b2} (c) ϕ_{b3}

(d) Total Biomass (e) AHL (f) ϕ_p

Figure 3: Biofilm development with both QS and non-QS bacteria in the biofilm system. The numerical simulation begins with 90% QS bacteria and 10% non-QS bacteria among all bacteria whose volume fraction is 2%. Four values of the growth rate for down-regulated QS bacteria C_{b1} are tested: $C_{b1} = 8 \times 10^{-5}$, 2×10^{-4}, 4×10^{-4} and 8×10^{-4} with $\beta = 0$. The corresponding volume fraction for each component is shown in the figure. (a) The volume fraction of QS-down regulated bacteria, where a rapid growth occurs initially, it is followed by a mild decay in a plateau, then a rapid decay, and finally the volume fraction settles down to a near steady state; (b) the volume fraction of QS-up regulated bacteria, which increases monotonically; (c) the volume fraction of non-QS bacteria, which increases rapidly to a steady state value; (d) the volume fraction of the total biomass (sum of the volume fractions of bacteria and EPS); (e) the concentration of QS molecules, AHL; (f)the volume fraction of EPS. The simulation shows that the higher C_{b1} is, the faster QS bacteria grow, which suppresses the growth of non-QS bacteria and enables the total biomass to reach a steady state sooner. At a small value of C_{b1}, the growth of QS bacteria is slow which allows the reproduction of non-QS regulated bacteria to outgrow QS regulated bacteria eventually. In this case, it also delays the biomass to reach a steady state so that the entire process of forming a robust biofilm is slowed down.

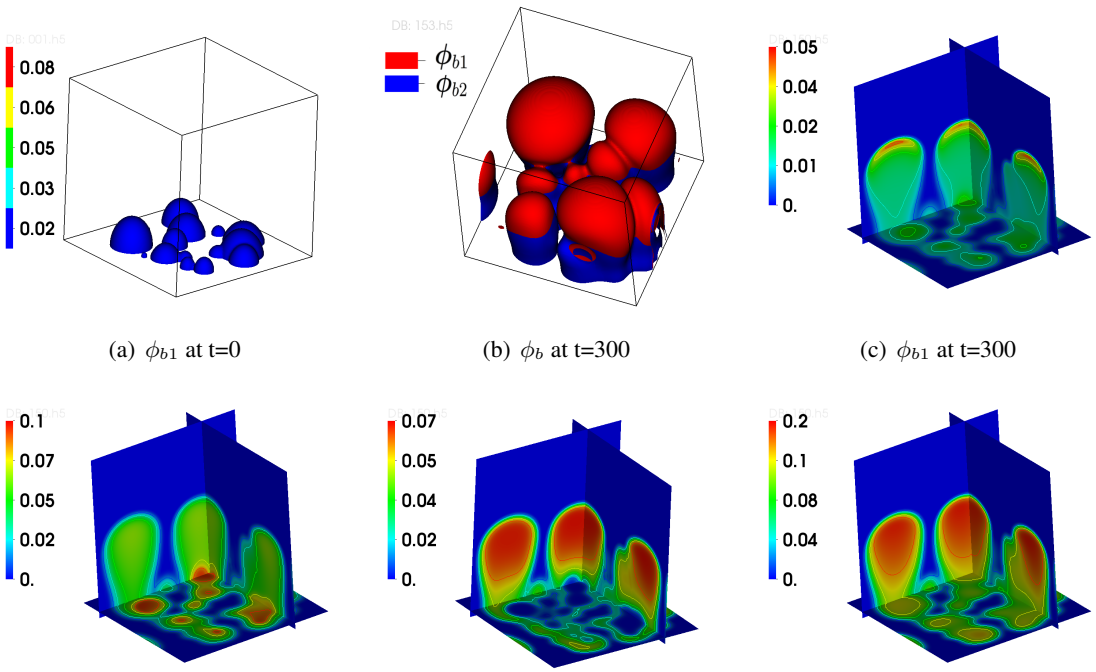

(a) ϕ_{b1} at t=0 (b) ϕ_b at t=300 (c) ϕ_{b1} at t=300

(d) ϕ_{b2} at t=300 (e) ϕ_p at t=300 (f) ϕ_n at t=300

Figure 4: Biofilm formation with EPS production coordinated by quorum sensing in the biofilm system where non QS bacteria are neglected. This simulation shows several clusters of QS^- in a developing heterogenous biofilm colony, where EPS production during biofilm formation is coordinated by quorum sensing. The initial profile is shown in (a). The characteristic time scale used is $t_0 = 10^3$ seconds and the simulation is conducted from $t = 0$ to $t = 300$, which represents roughly 3.4 days in real time. (b). A time $t = 300$, the bacterial distribution in terms of volume fractions is shown, where the red represents QS^- and the blue represents QS^+; they are mixed. In the result, more QS^+ are observed in the bulk of the biofilm while more QS^- show up near the biofilm surface. In (c)-(f), three 2D slices of QS^-, QS^+, EPS and the total biomass at $t = 300$ are depicted, respectively, from which more interior details of the biofilm colony are on display.

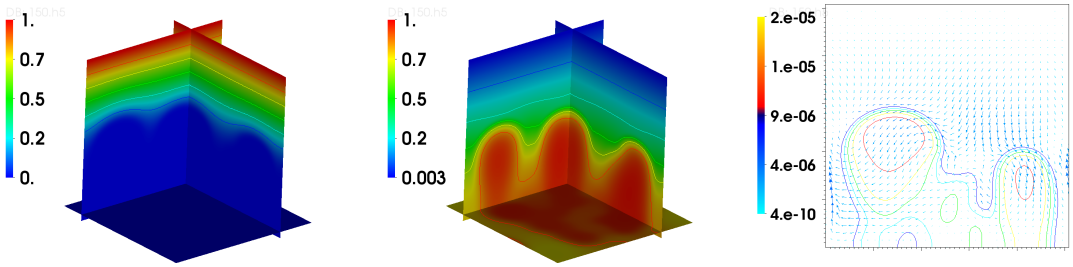

(a) Nutrient at t=300 (b) AHL at t=300 (c) $\mathbf{v}$ at t=300

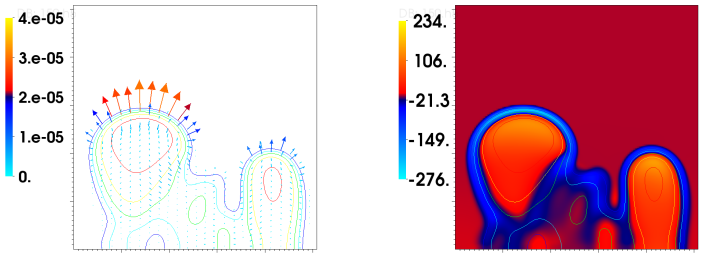

(d) $\phi_n \mathbf{v}_n$ at t=300 (e) Pressure at $t = 300$

Figure 5: Velocity, pressure and functional molecules from the simulation shown in Figure **??**. (a)-(b) 2D slices for the distribution of the nutrient and QS molecules, AHL; (c)-(e) 2D slice at $z = 0.5$ for the average velocity $\mathbf{v}$ and the biomass flux as well as the hydrostatic pressure at $t = 300$, respectively. Low pressures occur in the interfacial region where the biofilm tends to grow. (d) depicts explicitly the biomass flux given by $\phi_n \mathbf{v}_n$. This shows that QS molecules, AHL, are mainly concentrated in the biofilm colony, but, small amount is diffused into the surrounding environment.

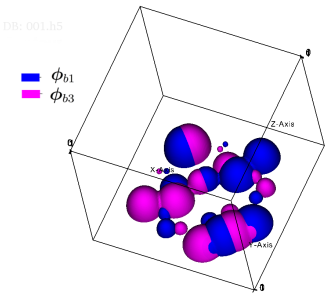

(a) Initial Condition

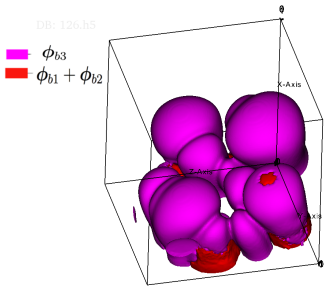

(b) Bacteria at t=252

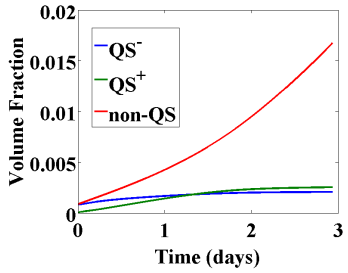

(c) Volume fractions for each bacterial type

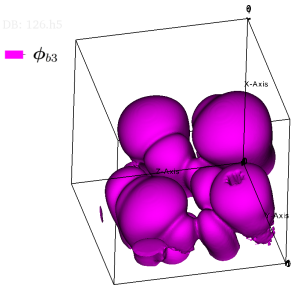

(d) ϕ_{b3} at t=252

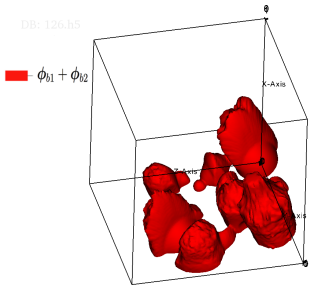

(e) ϕ_{b1} and ϕ_{b2} at t=252

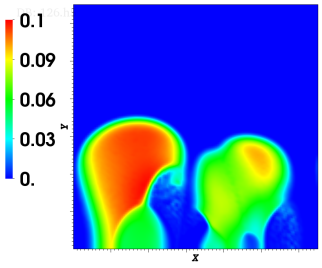

(f) ϕ_{b3} at t=252

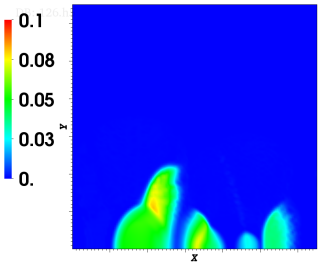

(g) ϕ_{b1} and ϕ_{b2} at t=252

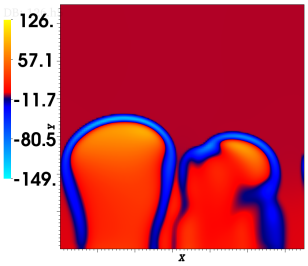

(h) Pressure at t=252

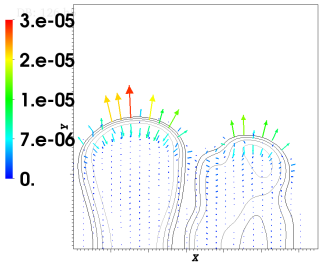

(i) Biomass flux $\phi_n \mathbf{v}_n$ at t=252

Figure 6: Biofilm development with both QS bacteria and Non-QS bacteria in the biofilm system. Randomly distributed biofilm colonies of multiple bacterial types are given initially. Here the characteristic time is set at $t_0 = 10^3$ seconds. (a) Initial bacterial volume fraction profiles; (b) bacterial volume fractions at time $t = 252$, where purple represents non-QS bacteria and red represents QS-bacteria; (c) the volume fraction for each bacterial phenotype in the entire biofilm colony, where non QS regulated bacteria outgrow the QS regulated bacteria; (d)the volume fraction of non QS bacteria; (e) the volume fraction of QS bacteria at $t = 252$; (f)-(i) 2D slices at $z = 0.5$ for non-QS, QS bacteria, hydrostatic pressure, and biomass flux $\phi_n \mathbf{v}_n$ at $t = 252$, respectively. The non QS regulated bacteria outgrow the QS regulated bacteria in most part of the biofilm except in regions near the bottom of the domain. The pressure is again small near the interface and large in the interior of the biofilm.

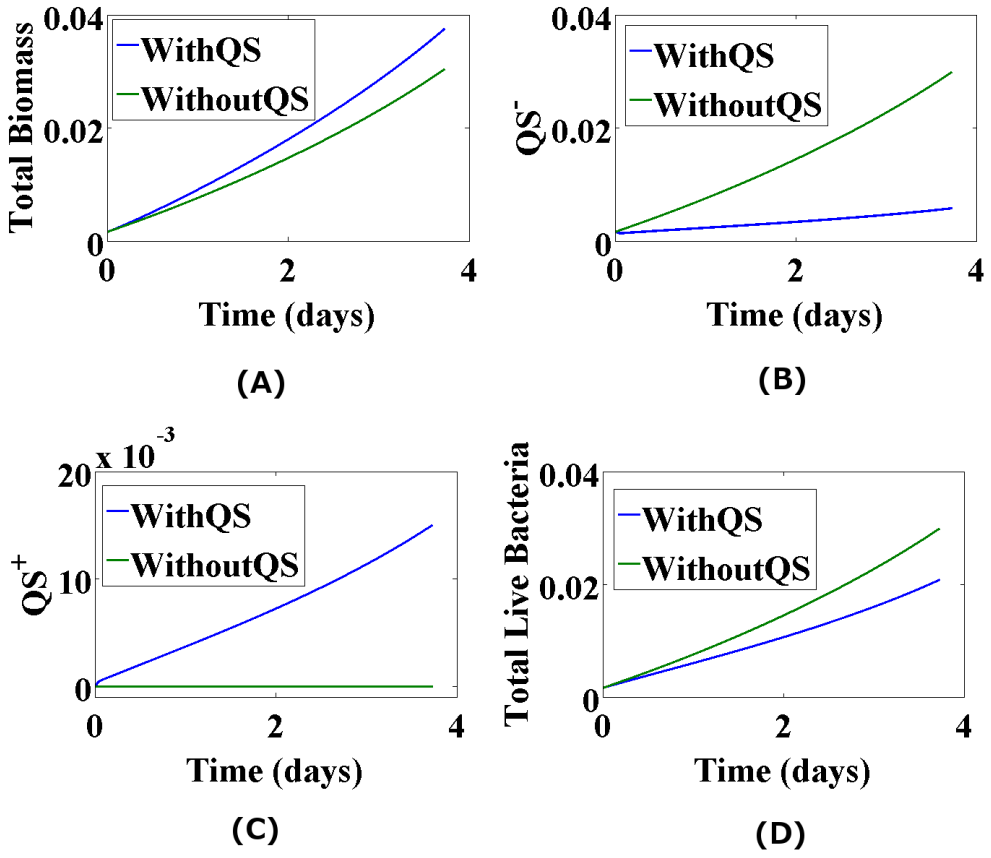

Figure 7: Comparison between bacterial volume fractions during biofilm development for biofilms with and without quorum sensing. Here we set $r_{12} = r_{21} = 0$ for simplicity. (a). Volume fractions of total biomass. (b). Volume fractions of QS down-regulated bacteria. (c). Volume fractions of QS up-regulated bacteria. (d). Volume fractions of total live bacteria. The initial conditions are the same as the one used in Figure **??**. With quorum sensing, the total biomass is higher than without quorum sensing, but the total live bacteria is not necessary be higher.

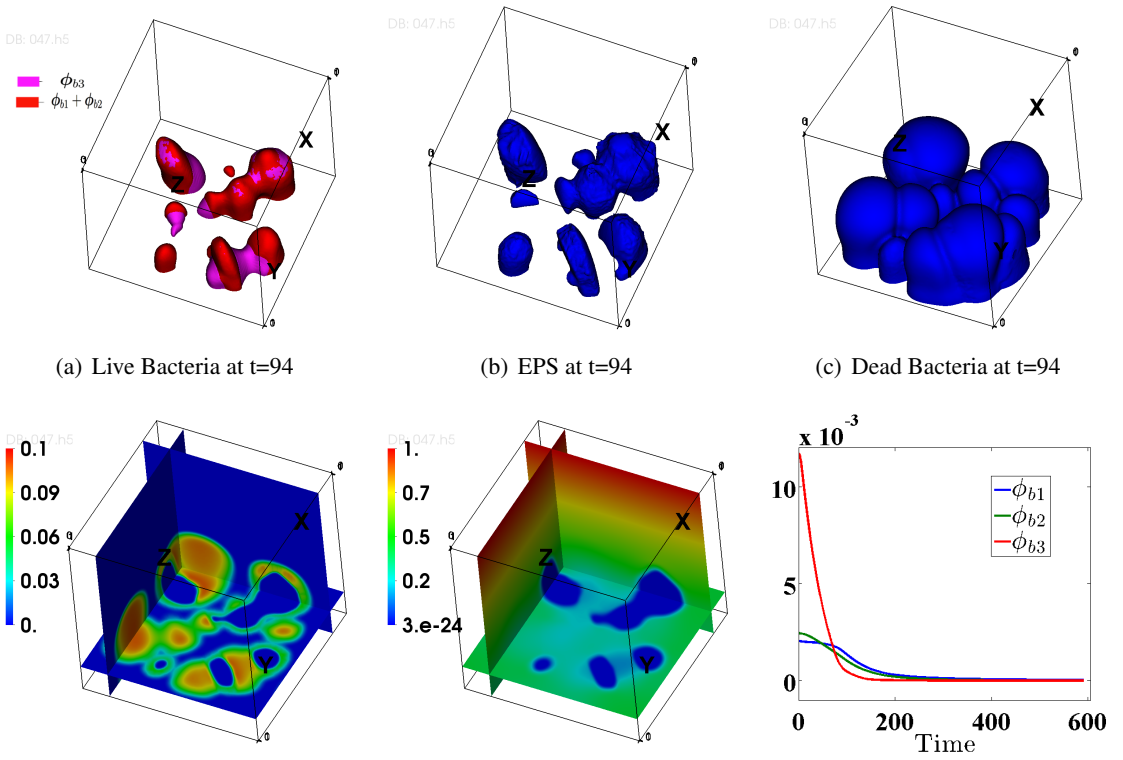

(a) Live Bacteria at t=94 (b) EPS at t=94 (c) Dead Bacteria at t=94

(d) Three Slices of ϕ_{b4} at t=94 (e) Three Slices of Drug at t=94 (f) Total Volume for Each Phenotypes

Figure 8: Biofilm development subject to both quorum sensing and antibiotic (drug) treatment. The initial biofilm profile is a grown biofilm at $t = 252$ from Figure **??**. Antibiotic agents are dosed from the top boundary. Here the characteristic time is $t_0 = 10$ seconds. (a)-(c) shows the volume fraction distribution of the live bacteria, EPS, dead bacteria at $t = 94$, respectively; (d)-(e) shows three slices of dead bacteria and antibiotics (drug) at $t = 94$, respectively; (f) shows total volume fractions of QS bacteria and non-QS bacteria from $t = 0$ to $t = 600$, respectively. After a long period of antibiotic treatment, the bacterial population is reduced to a negligible level in this simulation.

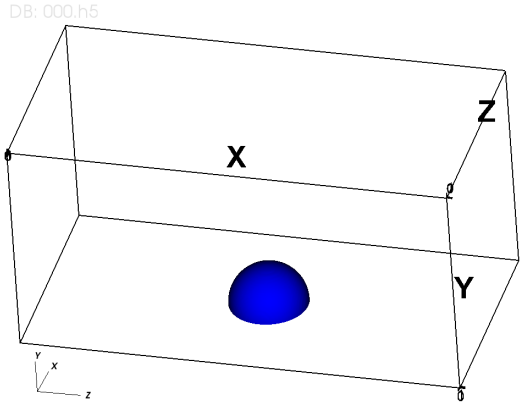

(a) Initial Condition ϕ_{b1}

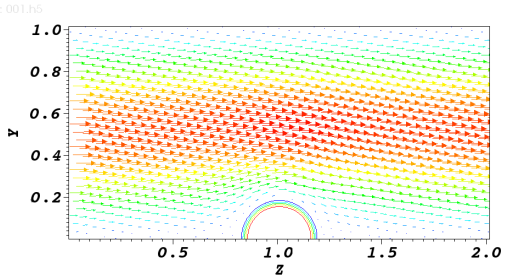

(b) Initial velocity $\mathbf{v}$ at $z = 0.5$

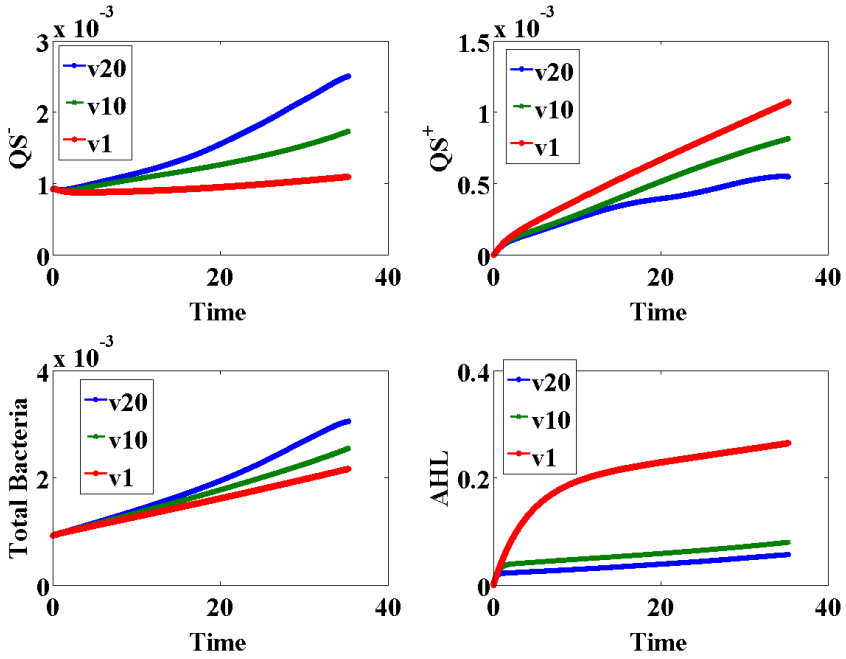

(c) Total volumes of each components

Figure 9: Biofilm development under different inlet flow velocities. This shows a comparative study on how some QS^- bacteria develop into a biofilm colony under different inlet velocities or equivalently inlet pressure gradients, i.e. $v_0 = p_0 y(1-y)$, where $p_0 = 1, 10, 20$. (a) The initial distribution of QS^- bacteria shown in volume fractions; (b) 2D slice ($z = 0.5$) of the initial velocity profile; (c) volume fractions of QS^- bacteria, QS^+ bacteria, total bacteria, as well as the concentration of AHL, at three selected inlet velocities. The volume fraction of QS^- bacteria and the total bacteria scales with the inlet speed, i.e., the higher the inlet speed is, the larger the volume fractions are; whereas the volume fraction of QS^+ bacteria and the AHL concentration scales inversely with the inlet speed, i.e., the larger the inlet speed is, the smaller the volume fraction and the concentration are.

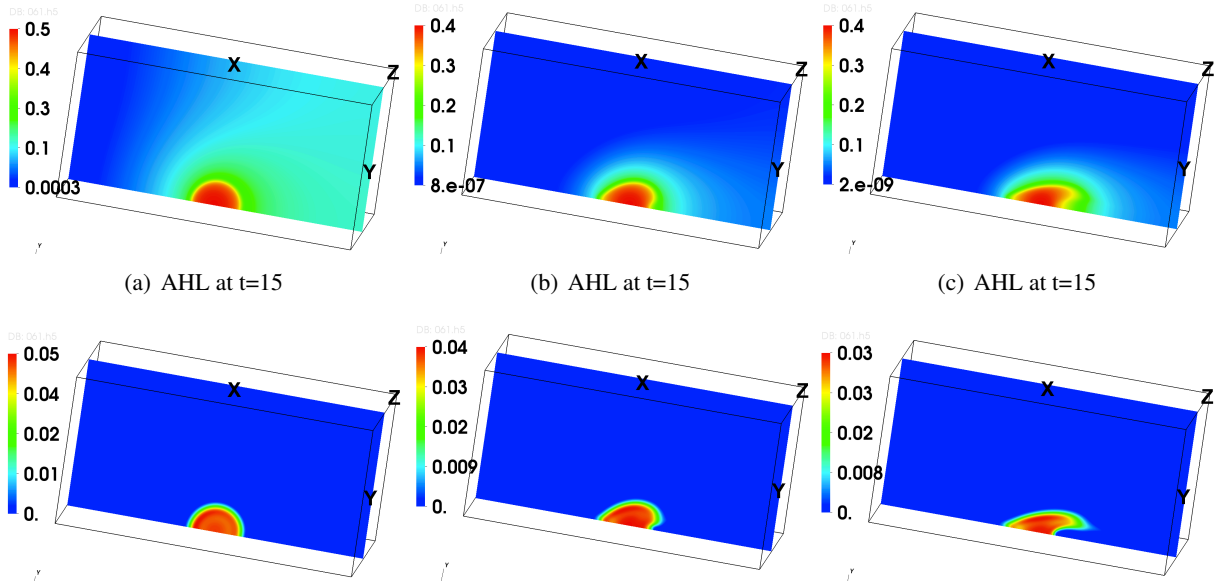

(a) AHL at t=15 (b) AHL at t=15 (c) AHL at t=15

(d) ϕ_{b2} at t=15 (e) ϕ_{b2} at t=15 (f) ϕ_{b2} at t=15

Figure 10: The volume fraction of QS^+ and AHL concentration at $t = 15$ with respect to three selected inlet speeds. This figure shows 2D slices at $z = 0.5$ for the simulation depicted in Figure **??**. (a)-(c) AHL concentration distribution at $t = 15$ for inlet velocity $v_0 = p_0 y(1 - y)$ with $p_0 = 1, 10, 20$, respectively; (d)-(f) 2D slice of the volume fraction of QS^+ (ϕ_{b2}) at $t = 15$ for inlet velocity $v_0 = p_0 y(1 - y)$ with $p_0 = 1, 10, 20$, respectively.

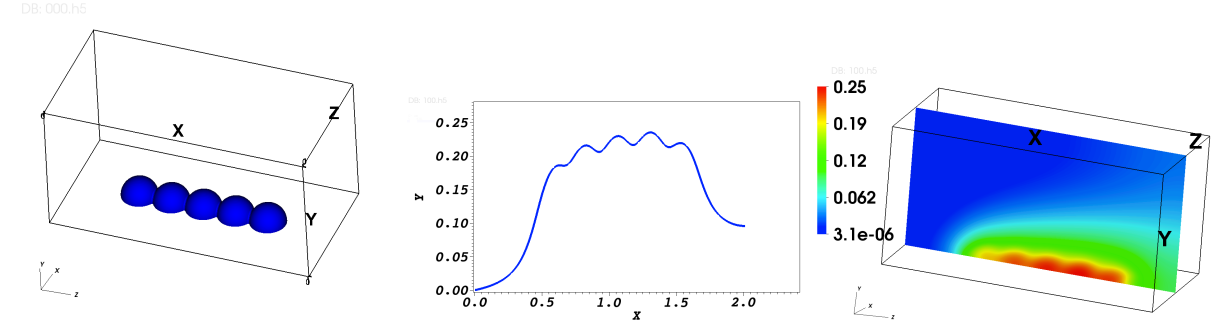

(a) Initial Condition (b) AHL at $x = 0.5$, $y = 0.0625$, t=25 (c) AHL at t=25

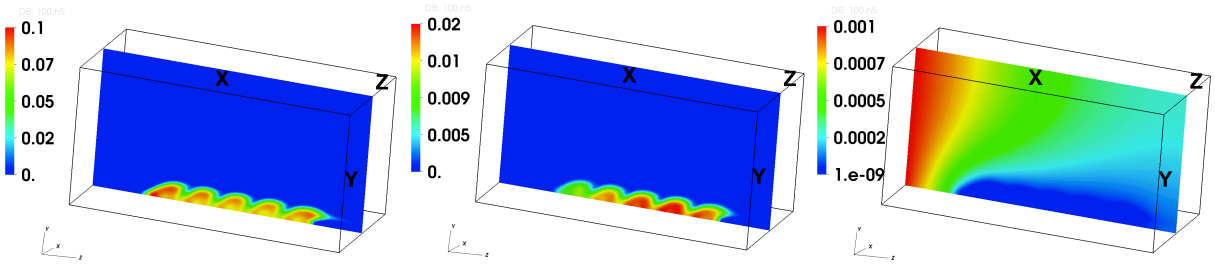

(d) ϕ_{b1} at t=25 (e) ϕ_{b2} at t=25 (f) Nutrient at t=25

Figure 11: Quorum sensing induction under hydrodynamic stress with a weak nutrient supply. This figure shows quorum sensing induction in a flow cell with an inlet flow velocity. In this simulation, $c_0 = 0.001$, representing a scenario with a weak nutrient supply. Initially some QS^- bacteria are attached to the substrate in the middle of the flow cell. (a) The initial profile of the QS^- bacteria; (b)AHL concentration at $x = 0.5$, $y = 0.0625$ and t=25; (c)-(f) 2D slices at $z = 0.5$ for AHL, ϕ_{b1}, ϕ_{b2}, as well as nutrient, distribution at time $t = 200$, respectively. When nutrient supplies are weak in the entire flow field, QS induction is stronger downstream than upstream. Consequently, there exist more QS^+ bacteria downstream than upstream.

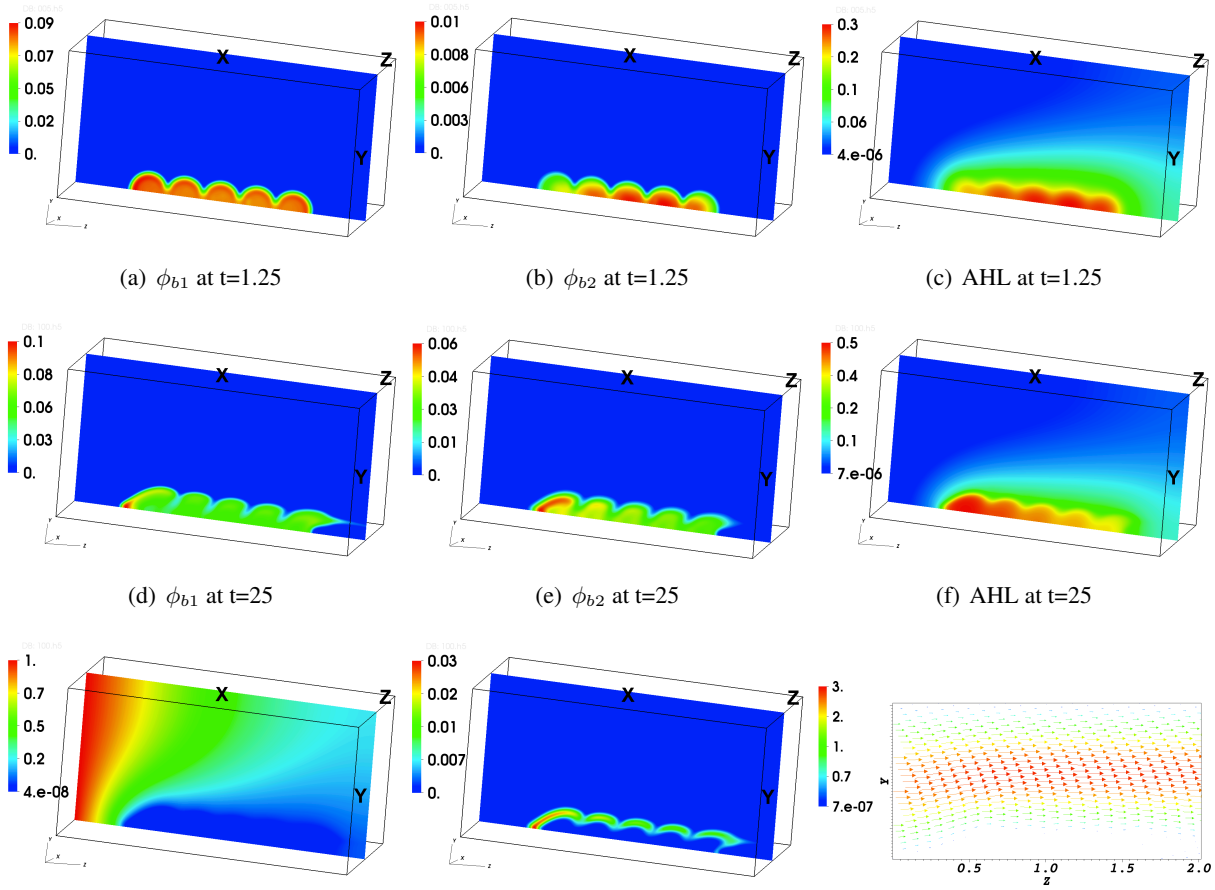

(a) ϕ_{b1} at t=1.25 (b) ϕ_{b2} at t=1.25 (c) AHL at t=1.25

(d) ϕ_{b1} at t=25 (e) ϕ_{b2} at t=25 (f) AHL at t=25

(g) Nutrient at t=25 (h) EPS at t=25 (i) $\mathbf{v}$ at t=25

Figure 12: Quorum sensing induction under hydrodynamic flow with a strong nutrient supply. This figure shows quorum sensing induction in a flow cell with inlet velocity $v_0 = 10y(1-y)$ and a strong nutrient supply ($c_0 = 1.0$). In this simulation we use the same initial distribution of QS^- as used in Figure **??** and characteristic time $t_0 = 10^3$ seconds. (a)-(c) show the 2D slices of the volume fraction of QS^- bacteria, QS^+ bacteria and the concentration of AHL at $z = 0.5$ and $t = 1.25$, respectively. (d)-(i). depict the volume fraction of QS^- bacteria, QS^+ bacteria, the concentration of AHL, the concentration of nutrient, the volume fraction of EPS, and the velocity field at $z = 0.5$ and $t = 25$, respectively. In this case, the strong nutrient supply dominates the growth of bacteria so that QS^+ grows the fastest near the upstream location than the downstream one.

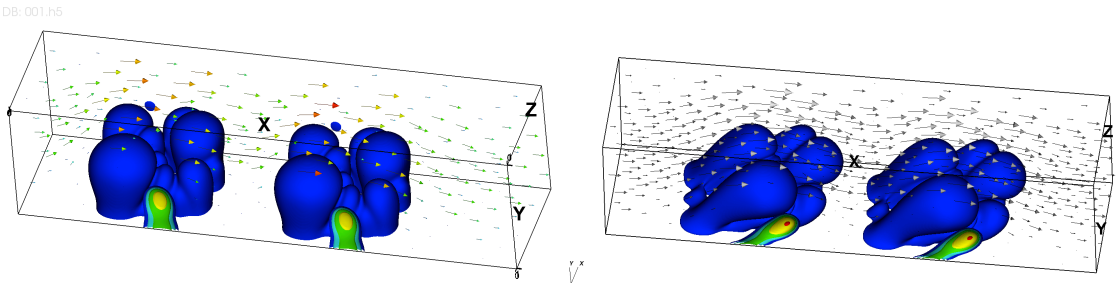

(a) ϕ_n at $t = 0$ (b) ϕ_n at $t = 31$

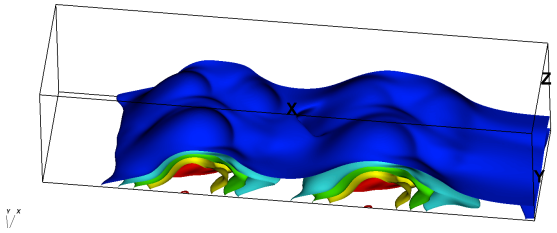

(c) AHL at $t = 31$

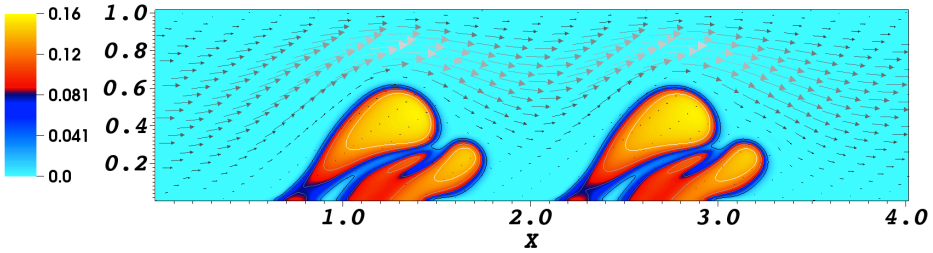

(d) 2D slice of ϕ_n at $z = 0.35$

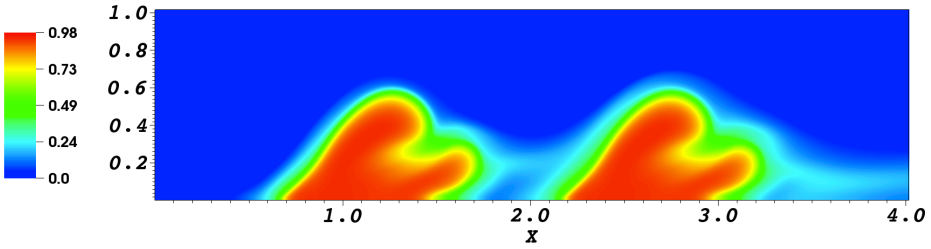

(e) 2D slice of AHL at $z = 0.35$

Figure 13: Hydrodynamic effects on biofilm morphology and the distribution of QS molecules. This figure shows two grown up biofilm colonies in a shear flow in a flow cell, where the characteristic time $t_0 = 1$ second. (a). The initial profile of the two biofilm colonies. (b). The two colonies at $t = 31$ in the shear flow. (c). Distribution of QS molecules, AHL. (d). A 2D slice of the biofilm colonies at $z = 0.35$ and $t = 31$. (e). A 2D slice of the AHL distribution at $z = 0.35$ and $t = 31$.

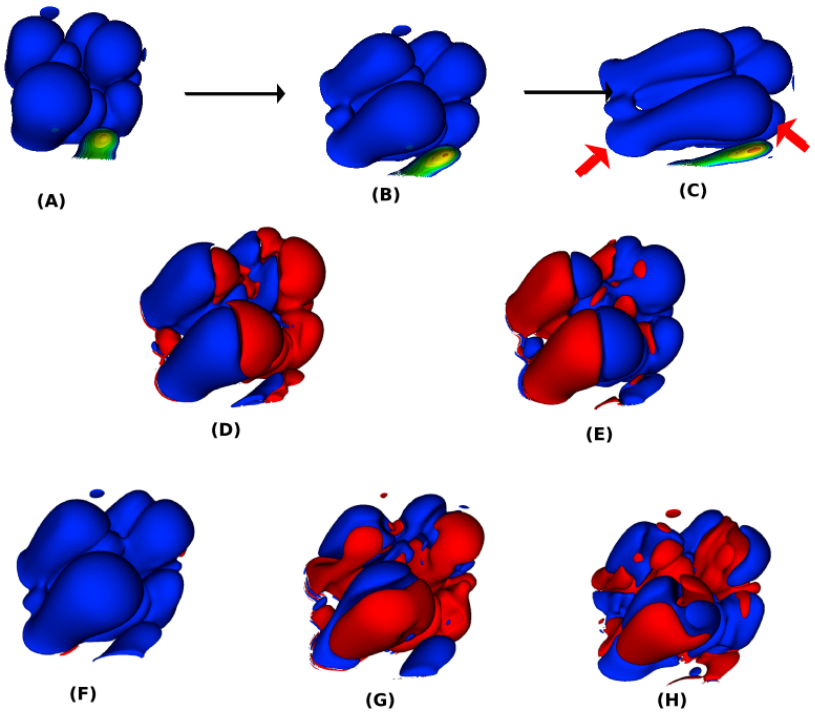

Figure 14: An anatomy of the hydrodynamic effect on biofilm morphology. (a)-(c) show the first biofilm colony in Figure (**??**) at time $t = 0, 18, 42$, respectively. We denote negative value by red and positive one by blue in the rest of the subfigures. The data shown are the solution at $t = 18$. (D) The second normal stress difference $N_1 = \phi_n(\tau_{yy} - \tau_{zz})$. (E) The first normal stress difference $N + 2 = \phi_n(\tau_{xx} - \tau_{yy})$. (F) The shear stress in xy plane $\phi_n\tau_{xy}$. (G) The shear stress in xz plane $\phi_n\tau_{xz}$. (H) The shear stress in yz plane $\phi_n\tau_{yz}$. The first and second normal stress difference are of opposite signs in most part of the colony. The primary shear stress $\phi_n\tau_{xy}$ is always positive while the two secondary shear stress components can take on either signs.